Innate αβ T Cells Mediate Antitumor Immunity by Orchestrating Immunogenic Macrophage Programming

Mautin Hundeyin[1], Emma Kurz[1], Ankita Mishra[1], Juan Andres Kochen Rossi[1], Shannon M. Liudahl[2], Kenna R. Leis[2], Harshita Mehrotra[1], Mirhee Kim[1], Luisana E. Torres[1], Adesola Ogunsakin[1], Jason Link[3,4], Rosalie C. Sears[3,4,5], Shamilene Sivagnanam[6], Jeremy Goecks[5,6], K.M. Sadeq Islam[1], Igor Dolgalev[7], Shivraj Savadkar[1], Wei Wang[1], Berk Aykut[1], Joshua Leinwand[1], Brian Diskin[1], Salma Adam[1], Muhammad Israr[1], Maeliss Gelas[1], Justin Lish[1], Kathryn Chin[1], Mohammad Saad Farooq[1], Benjamin Wadowski[1], Jingjing Wu[1], Suhagi Shah[8], Dennis O. Adeegbe[8], Smruti Pushalkar[9], Varshini Vasudevaraja[7], Deepak Saxena[9], Kwok-Kin Wong[8], Lisa M. Coussens[2,4,5], and George Miller[1,10]

ABSTRACT

Unconventional T-lymphocyte populations are emerging as important regulators of tumor immunity. Despite this, the role of $TCR\alpha\beta^+CD4^-CD8^-NK1.1^-$ innate αβ T cells (iαβT) in pancreatic ductal adenocarcinoma (PDA) has not been explored. We found that iαβTs represent ~10% of T lymphocytes infiltrating PDA in mice and humans. Intratumoral iαβTs express a distinct T-cell receptor repertoire and profoundly immunogenic phenotype compared with their peripheral counterparts and conventional lymphocytes. iαβTs comprised ~75% of the total intratumoral $IL17^+$ cells. Moreover, iαβT-cell adoptive transfer is protective in both murine models of PDA and human organotypic systems. We show that iαβT cells induce a CCR5-dependent immunogenic macrophage reprogramming, thereby enabling marked $CD4^+$ and $CD8^+$ T-cell expansion/activation and tumor protection. Collectively, iαβTs govern fundamental intratumoral cross-talk between innate and adaptive immune populations and are attractive therapeutic targets.

SIGNIFICANCE: We found that iαβTs are a profoundly activated T-cell subset in PDA that slow tumor growth in murine and human models of disease. iαβTs induce a CCR5-dependent immunogenic tumor-associated macrophage program, T-cell activation and expansion, and should be considered as novel targets for immunotherapy.

See related commentary by Banerjee et al., p. 1164.

---

[1] S.A. Localio Laboratory, Department of Surgery, New York University School of Medicine, New York, New York. [2] Department of Cell, Developmental and Cancer Biology, Oregon Health and Science University, Portland, Oregon. [3] Department of Molecular and Medical Genetics, Oregon Health and Science University, Portland, Oregon. [4] Brenden-Colson Center for Pancreatic Care, Oregon Health and Science University, Portland, Oregon. [5] Knight Cancer Institute, Oregon Health and Science University, Portland, Oregon. [6] Computational Biology Program, Oregon Health and Science University, Portland, Oregon. [7] Department of Pathology, New York University School of Medicine, New York, New York. [8] Department of Medicine, New York University School of Medicine, New York, New York. [9] Department of Basic Science and Craniofacial Biology, New York University College of Dentistry, New York, New York. [10] Department of Cell Biology, New York University School of Medicine, New York, New York.

Note: Supplementary data for this article are available at Cancer Discovery Online (http://cancerdiscovery.aacrjournals.org/).

M. Hundeyin and E. Kurz share first authorship of this article.

Corresponding Author: George Miller, New York University School of Medicine, 435 East 30th Street, 4th Floor, NSB, New York, NY 10016. Phone: 201-446-3608; Fax: 646-501-2208; E-mail: george.miller@nyumc.org

Cancer Discov 2019;9:1288–305

doi: 10.1158/2159-8290.CD-19-0161

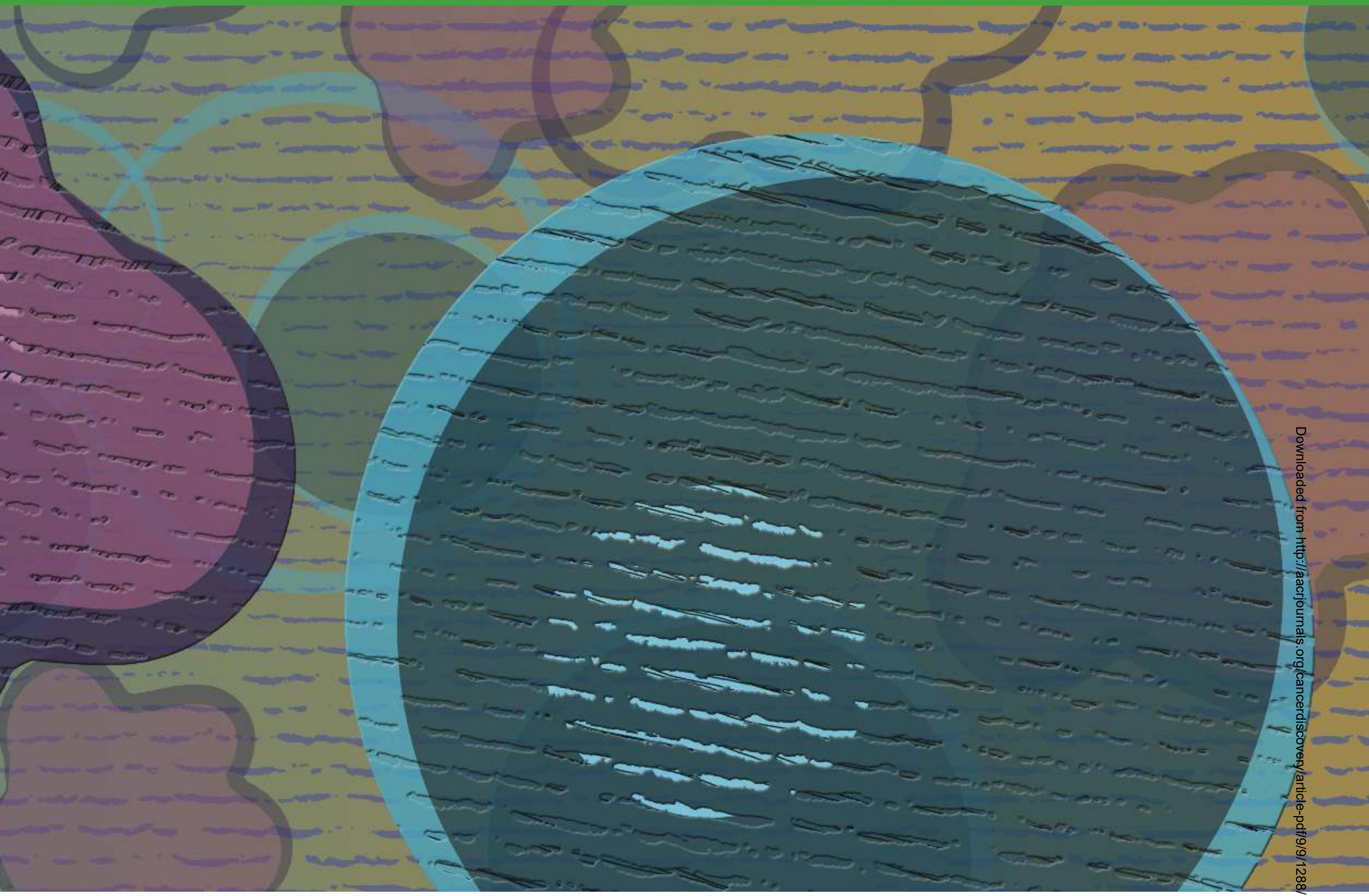

INTRODUCTION

The phenotypic composition of inflammatory cells infiltrating pancreatic ductal adenocarcinoma (PDA) influences disease outcome (1). Depending on the signals released, innate immune cells entrain the adaptive immune compartment toward an immunogenic or tolerogenic response, affecting PDA growth and metastasis. Classically activated M1-like macrophages secrete proinflammatory mediators, such as TNFα, IFNγ, and IL12, which in turn polarize $CD4^+$ T cells toward a Th1 phenotype and activate cytotoxic $CD8^+$ T cells. More commonly, alternatively activated M2-like macrophages promote tolerogenic Th2 and T regulatory cell (Treg) differentiation (2). However, this relationship is bidirectional, as adaptive immune cells can in turn influence innate immune programming. For example, we previously showed that $CD4^+$ T cells can augment tolerogenic macrophage polarization via IL4 (3). Similarly, $FOXP3^+$ Tregs can influence dendritic cell capacity for cross-presentation of tumor antigen (4). These data suggest bidirectional cross-talk between innate and adaptive immune subsets in the PDA tumor microenvironment (TME).

There is growing evidence illustrating the contribution of unconventional T lymphocytes in shaping the immune milieu in PDA. γδT cells, characterized by expression of TCRγδ, expand early in pancreatic oncogenesis. We showed that γδT cells exert direct immune-suppressive influences on conventional T cells in PDA via the PD-L1–PD-1 axis (5). By contrast, natural killer T cells (NKT cells) have recently been shown to protect against PDA by modulating the phenotype of tumor-associated macrophages (TAM) through mPGES-1 and 5-LOX (6).

We observed that $CD3^+TCR\alpha\beta^+CD4^-CD8^-NK1.1^-$ cells represented ~10% of T cells in murine and human PDA. Given the emerging role for unconventional T cells in PDA, we were spurred to investigate the function of these iαβTs in this disease. iαβTs exhibited a unique cellular program that was influenced by diverse microbial and sterile stimuli within the TME. We further hypothesized that iαβTs may have important immune-modulatory functions in PDA. We found that iαβTs exhibited marked tumor-protective properties in both murine and human PDA by driving a CCR5-dependent immunogenic macrophage polarization, resulting in conventional T-cell activation *in situ*. Collectively, our work uncovers fundamental intratumoral cross-talk between iαβTs and the innate and adaptive immune compartments, and suggests that strategies targeting iαβTs may be effective for reprogramming of the TME in human cancer.

RESULTS

iαβTs Are a Prominent T-cell Population in Murine and Human PDA

To assess the significance of iαβTs in PDA, we determined their prevalence in an invasive orthotopic model of PDA using tumor cells derived from *Pdx1*$^{\text{Cre}}$;*Kras*$^{\text{G12D}}$;*Trp53*$^{\text{R172H}}$ (KPC) mice that express mutant *Kras* and *Trp53* in their pancreatic progenitor cells, a slowly progressive preinvasive autochthonous model of PDA using *p48*$^{\text{Cre}}$;*Kras*$^{\text{G12D}}$ (KC) mice whose pancreata express oncogenic *Kras* alone, and human disease. We discovered that CD4$^-$CD8$^-$NK1.1$^-$ iαβTs constitute ~10% of TCRαβ$^+$ T cells in orthotopic KPC tumors (Fig. 1A; Supplementary Fig. S1a) and KC pancreata (Fig. 1B). Human PDA similarly possessed an increased CD4$^-$CD8$^-$ T-cell infiltrate compared with normal adjacent pancreas or peripheral blood mononuclear cells (PBMC; Fig. 1C; Supplementary Fig. S1b). By contrast, iαβTs were scarce in murine spleen and human PBMCs. PDA-infiltrating iαβTs did not express characteristic functional markers of NKT cells and ~10% bound an MR1-specific tetramer, compared with ~40% in the gut (Supplementary Fig. S1c-f). Single-cell RNA sequencing (RNA-seq) of PDA-infiltrating CD3$^+$ cells further confirmed that this population is transcriptomically distinct from CD4$^+$, CD8$^+$, γδT, and NKT cell populations (Fig. 1D). iαβTs upregulated *Ccr7* expression and exhibited reduced *Il2rb* in comparison with other lymphocyte populations (Supplementary Fig. S1g and h). These observations were confirmed by flow cytometry (Supplementary Fig. S1i and j). In-depth analysis comparing iαβT with NKT cells revealed that iαβT cells downregulated the NKT markers *Klrk1, Klra7, Klrd1, NKG7, Klrc2*, and *Ly6c2* but upregulated the transcription factors *Socs3* and *Junb* (Supplementary Fig. S1k). Interestingly, iαβTs increased as a fraction of TCRαβ$^+$CD4$^-$CD8$^-$ T cells as tumors progressed (Fig. 1E). γδT cells remained stable over the course of oncogenesis, as previously reported (1). Multiplex IHC suggested that iαβTs were interspersed among CD4$^+$ and CD8$^+$ T cells within the TME (Fig. 1F). Of note, PDA-infiltrating iαβTs constituted ~30% of TCRαβ$^+$ cells in *Fas*$^{\text{lpr}}$ mice (Fig. 1G), known to accumulate iαβTs in secondary lymphoid organs (7). To determine whether the thymic production of iαβTs is accelerated during pancreatic oncogenesis, we interrogated T-cell populations in the thymus of 6-month-old KC mice. Thymic iαβTs were not increased in prevalence in KC mice compared with wild-type (WT; Fig. 1H). Adoptive transfer tracking experiments suggested that neither CD4$^+$ nor CD8$^+$ T cells converted to the iαβT phenotype in PDA. Likewise, iαβTs did not gain CD4 or CD8 expression (Fig. 1I). Interestingly, cellular proliferation was higher in PDA-infiltrating iαβTs than in either CD4$^+$ or CD8$^+$ T cells (Fig. 1J). We recently reported that unconventional T cells, particularly γδT cells, are recruited to the PDA TME via diverse chemokine signaling networks (5). We observed that PDA-infiltrating iαβTs express CCR2, CCR5, and CCR6 (Fig. 1K), and CCR2 deletion trended to mitigate iαβT recruitment in PDA (Fig. 1L).

iαβTs Exhibit a Distinctive Phenotype in PDA and Are Targets of Immunotherapy

PDA-infiltrating iαβTs acquire a distinctive phenotype relative to the periphery. Tumor-penetrating iαβT expressed the adhesion ligand JAML and the cytotoxic marker CD107a (Fig. 2A and B). Additionally, iαβTs in the TME upregulated the checkpoint receptors CTLA4, TIM3, PD-1, and LAG3, ectonucleotidases CD39 and CD73, costimulatory receptors CD40L and ICOS, and the C-type lectin receptor Dectin-1 (Fig. 2C–G). PDA-associated iαβTs were also highly activated compared with their splenic counterparts, downregulating CD62L (Fig. 2H). Moreover, the T-cell receptor (TCR) nucleotide sequences of tumor-infiltrating iαβTs exhibited minimal overlap with those of splenic iαβTs or conventional T cells infiltrating PDA (Fig. 2I; Supplementary Table S1). iαβTs in the TME were further distinct from both intratumoral CD4$^+$ and CD8$^+$ T cells and splenic iαβT in their high expression of the Th1-family transcription factor T-bet (Fig. 2J). STAT1 signaling, associated with Th1 differentiation, was similarly upregulated in iαβTs in PDA (Supplementary Fig. S2a). Expression of the Th17-family transcription factor RORγt was also increased (Supplementary Fig. S2b). Accordingly, PDA-infiltrating iαβTs expressed high IFNγ and TNFα compared to their splenic counterparts and to both intratumoral CD4$^+$ and CD8$^+$ T cells (Supplementary Fig. S2c and d). IFNγ and IL17 were distinctively coexpressed in the iαβT-cell

Figure 1. iαβTs expand in PDA. **A,** CD45$^+$ leukocytes infiltrating day 21 orthotopic KPC tumors, normal pancreas (panc), and spleens in WT mice were gated and tested for the frequency of TCRβ$^+$CD4$^-$CD8$^-$NK1.1$^-$ iαβTs. Representative contour plots and quantitative data are shown ($n = 10$). **B,** CD45$^+$TCRβ$^+$NK1.1$^-$ leukocytes from pancreata and spleens of 6-month-old KC mice were gated and tested for coexpression CD4 and CD8. Representative contour plots are shown ($n = 5$). **C,** Multiplex IHC of human PDA and adjacent normal (nml) pancreas were stained for CK19, CD3, CD4, and CD8. The frequency of CD3$^+$CD4$^-$CD8$^-$ cells was quantified, and representative images are shown. Scale bars, 5 μm. **D,** Orthotopic KPC tumors were harvested from WT mice on day 21. CD45$^+$CD3$^+$ leukocytes were purified by FACS and analyzed by single-cell RNA-seq. The distribution of cellular clusters was determined using the t-SNE algorithm. Each cluster is identified by a distinct color. Percent cellular abundance in each cluster is indicated. **E,** Orthotopic KPC tumors were harvested from WT mice on day 7, 14, or 21 after tumor cell implantation, and tumor-infiltrating CD45$^+$TCRβ$^+$CD4$^-$CD8$^-$ leukocytes were gated and tested for expression of NK1.1. Representative contour plots from days 7 and 21 and quantitative data comparing frequency of tumor-infiltrating iαβT per NKT cells at all time points are shown ($n = 5$/time point). **F,** Paraffin-embedded sections made from tumors of mice serially treated with anti-TCRγ/δ and NK1.1 depleting antibodies were tested for coexpression of hematoxylin, CD3, CD4, and CD8 in the PDA TME. Scale bar, 5 μm. **G,** CD45$^+$TCRβ$^+$NK1.1$^-$ leukocytes infiltrating orthotopic KPC tumors in WT and *Fas*$^{\text{lpr}}$ mice were gated and tested for expression of CD4 and CD8. Representative contour plots and quantitative data are shown ($n = 5$/group). **H,** The thymus from 6-month-old WT and KC mice were harvested and CD45$^+$TCRβ$^+$ thymocytes were gated and tested for expression of CD4 and CD8. The frequency of iαβTs in the thymus was calculated ($n = 5$/group). **I,** CD4$^+$ T cells, CD8$^+$ T cells, or iαβTs were harvested from CD45.1 mice and transferred intravenously to orthotopic PDA-bearing CD45.2 mice. PDA tumors were harvested at 96 hours and CD45.1$^+$ cells were gated and tested for CD4 and CD8 expression. Representative contour plots are shown ($n = 5$/group). **J,** WT mice were orthotopically administered KPC tumor cells and sacrificed on day 21. PDA-infiltrating CD4$^+$ T cells, CD8$^+$ T cells, and iαβTs were assayed for Ki67 proliferative index. Representative contour plots and quantitative data are shown ($n = 5$). **K,** Splenic and orthotopic PDA-infiltrating iαβTs were tested on day 21 for expression of CCR2, CCR5, and CCR6 ($n = 5$). **L,** The frequency of PDA-infiltrating iαβTs was tested on day 21 in WT, CCR2$^{-/-}$, CCR5$^{-/-}$, and CCR6$^{-/-}$ hosts ($n = 5$/group). All experiments were repeated at least 3 times. *, $P < 0.05$; **, $P < 0.01$; ***, $P < 0.001$; ****, $P < 0.0001$. ns, not significant.

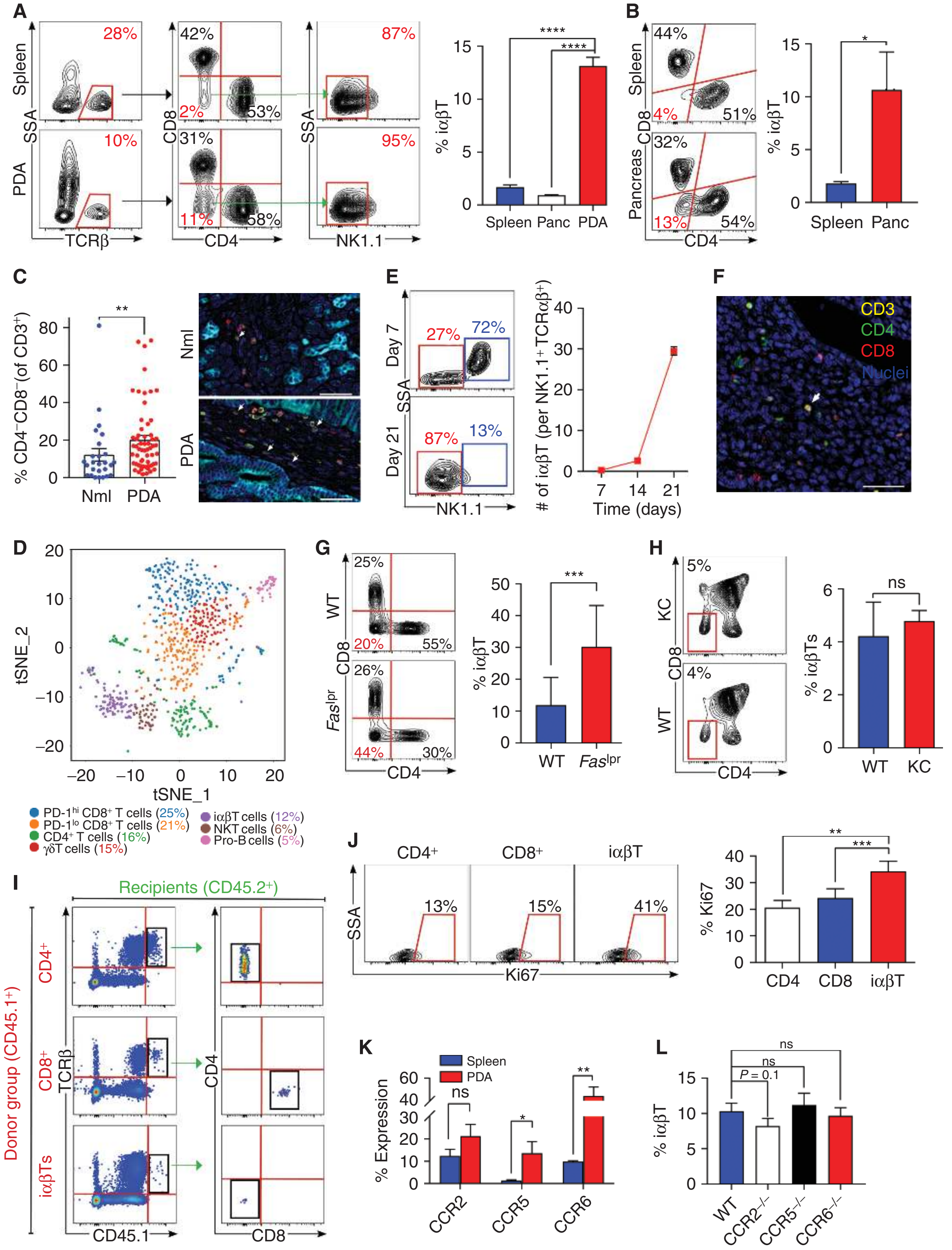
A
Spleen
PDA
SSA
TCRβ
28%
10%
42%
2%
53%
31%
11%
58%
CD8
CD4
87%
95%
SSA
NK1.1
% iαβT
15
10
5
0
****
****
Spleen
Panc
PDA
B
Spleen
Pancreas
CD8
CD4
44%
4%
51%
32%
13%
54%
% iαβT
*
Spleen
Panc
C
% CD4⁻CD8⁻(of CD3⁺)
80
60
40
20
0
**
Nml
PDA
Nml
PDA
E
Day 7
Day 21
SSA
NK1.1
27%
72%
87%
13%
# of iαβT (per NK1.1⁺ TCRαβ⁺)
40
30
20
10
0
7
14
21
Time (days)
F
CD3
CD4
CD8
Nuclei
D
tSNE_2
tSNE_1
20
10
0
−10
−20
PD-1hi CD8⁺ T cells (25%)
PD-1lo CD8⁺ T cells (21%)
CD4⁺ T cells (16%)
γδT cells (15%)
iαβT cells (12%)
NKT cells (6%)
Pro-B cells (5%)
G
WT
Faslpr
CD8
CD4
25%
20%
55%
26%
44%
30%
% iαβT
50
40
30
20
10
0
***
WT
Faslpr
H
KC
WT
CD8
CD4
5%
4%
% iαβTs
6
4
2
0
ns
WT
KC
I
Recipients (CD45.2⁺)
Donor group (CD45.1⁺)
CD4⁺
CD8⁺
iαβTs
TCRβ
CD45.1
CD4
CD8
J
CD4⁺
CD8⁺
iαβT
SSA
Ki67
13%
15%
41%
% Ki67
40
30
20
10
0
**
***
CD4
CD8
iαβT
K
Spleen
PDA
% Expression
60
40
30
20
10
0
ns
*
**
CCR2
CCR5
CCR6
L
% iαβT
15
10
5
0
ns
ns
P = 0.1
WT
CCR2⁻/⁻
CCR5⁻/⁻
CCR6⁻/⁻

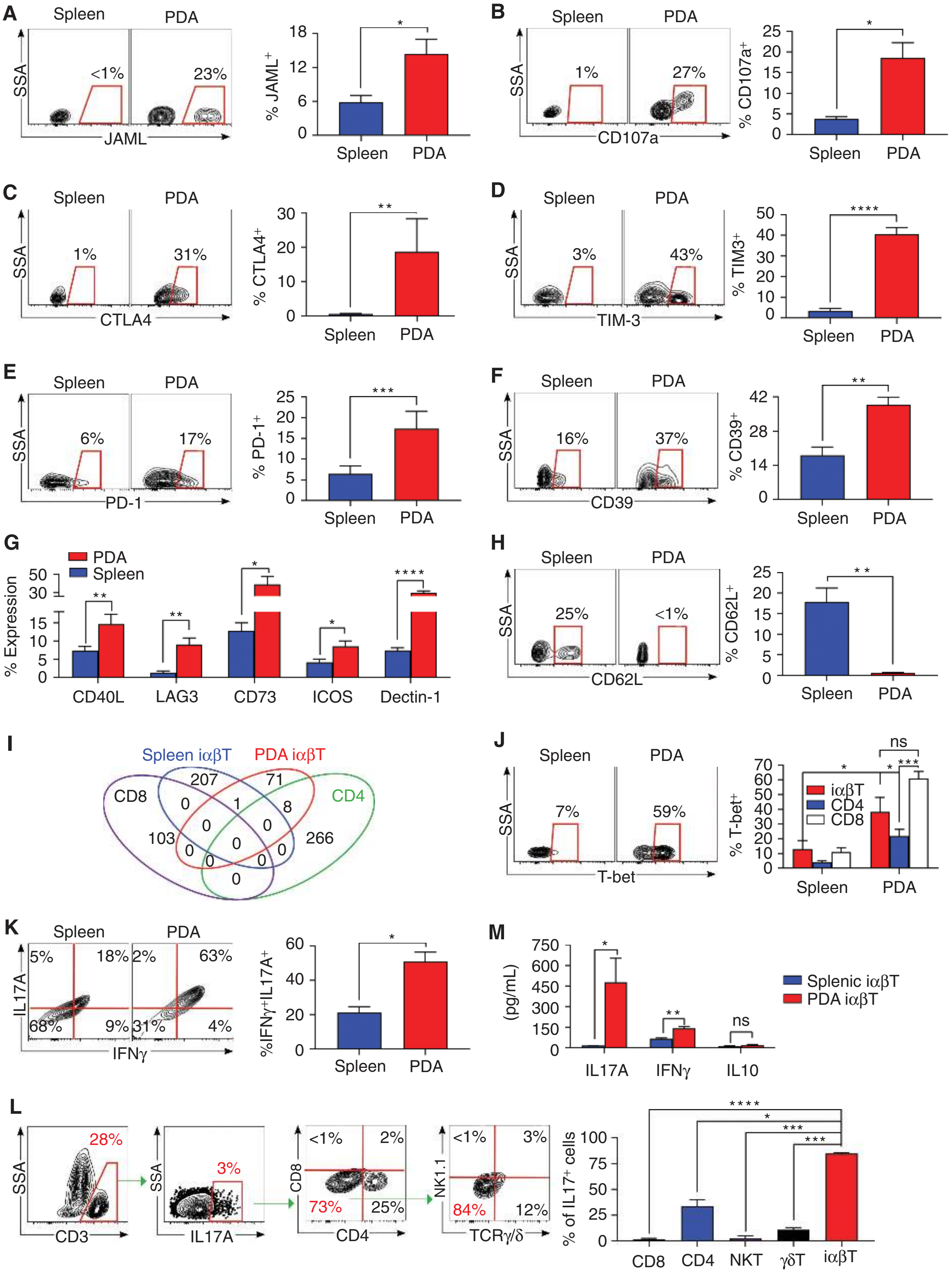
A
Spleen
PDA
SSA
<1%
23%
JAML
% JAML+
18
12
6
0
*
Spleen
PDA
B
Spleen
PDA
SSA
1%
27%
CD107a
% CD107a+
25
20
15
10
5
0
*
Spleen
PDA
C
Spleen
PDA
SSA
1%
31%
CTLA4
% CTLA4+
30
20
10
0
**
Spleen
PDA
D
Spleen
PDA
SSA
3%
43%
TIM-3
% TIM3+
50
40
30
20
10
0
****
Spleen
PDA
E
Spleen
PDA
SSA
6%
17%
PD-1
% PD-1+
25
20
15
10
5
0
***
Spleen
PDA
F
Spleen
PDA
SSA
16%
37%
CD39
% CD39+
42
28
14
0
**
Spleen
PDA
G
PDA
Spleen
% Expression
50
30
15
10
5
0
**
**
*
*
****
CD40L
LAG3
CD73
ICOS
Dectin-1
H
Spleen
PDA
SSA
25%
<1%
CD62L
% CD62L+
25
20
15
10
5
0
**
Spleen
PDA
I
Spleen iαβT
PDA iαβT
CD8
CD4
207
71
0
1
8
0
0
103
0
0
0
0
266
0
0
J
Spleen
PDA
SSA
7%
59%
T-bet
% T-bet+
70
60
50
40
30
20
10
0
ns
*
*
***
iαβT
CD4
CD8
Spleen
PDA
K
Spleen
PDA
IL17A
5%
18%
2%
63%
68%
9%
31%
4%
IFNγ
%IFNγ+IL17A+
60
40
20
0
*
Spleen
PDA
M
(pg/mL)
750
600
450
300
150
0
*
**
ns
IL17A
IFNγ
IL10
Splenic iαβT
PDA iαβT
L
SSA
28%
CD3
SSA
3%
IL17A
CD8
<1%
2%
73%
25%
CD4
NK1.1
<1%
3%
84%
12%
TCRγ/δ
% of IL17+ cells
100
75
50
25
0
****
*
***
***
CD8
CD4
NKT
γδT
iαβT

population (Fig. 2K). Notably, iαβTs in tumor accounted for ~75% of the total IL17$^+$ immune cells in PDA (Fig. 2L). By contrast, FOXP3 and IL10 were minimally expressed in iαβTs in PDA, whereas TGFβ was upregulated (Supplementary Fig. S2e–g). Analysis of iαβT cell–conditioned media confirmed high IL17 and IFNγ, but low IL10, secretion (Fig. 2M).

Immunotherapy has emerged as an efficacious treatment option in select subsets of patients with PDA (8). Because iαβTs express high levels of costimulatory molecules and checkpoint receptors in PDA, we postulated that immune-based therapies targeting these entities would activate iαβTs *in situ*. Accordingly, we found that ICOS ligation upregulated IFNγ and IL17 expression in splenic iαβTs *in vitro* (Supplementary Fig. S3a and b). Further, treatment of PDA-bearing mice with an ICOS agonist was tumor-protective and was associated with marked iαβT cellular expansion and activation (Supplementary Fig. S3c–e). Given our observation that PDA-infiltrating iαβTs upregulate PD-1, we also tested the effect of PD-L1 blockade on the iαβT phenotype (Fig. 2E). αPD-L1 mAb treatment promoted iαβT activation in the TME (Supplementary Fig. S3f). These data suggest that iαβTs are distinctive targets of costimulatory and checkpoint receptor based therapy in PDA whose impact must be considered in immune-based therapeutics. Moreover, the combination of αPD-L1 treatment and iαβT cell transfer offered additional protection compared with either monotherapy (Supplementary Fig. S3g).

To investigate whether PDA-infiltrating iαβTs are MHC I or MHC II restricted, we administered orthotopic PDA tumor to β2-microglobulin$^{-/-}$ and MHC II$^{-/-}$ mice, respectively. PDA tumors in MHC II$^{-/-}$ hosts did not alter iαβT-cell recruitment (Supplementary Fig. S3h), whereas β2-microglobulin–deficient mice exhibited reduced iαβT-cell recruitment to the PDA TME and lower cellular expression of T-bet and TNFα (Supplementary Fig. S3i–k). In contrast to CD8$^+$ T cells, however, iαβT-infiltrating Ova-expressing PDA tumors lacked Ova-pentamer staining and were thus not MHC I antigen restricted, lending support to their innate immune properties (Supplementary Fig. S3l and m). Accordingly, intratumoral iαβTs were less clonal than both CD4$^+$ and CD8$^+$ T cells (Supplementary Fig. S3n).

iαβT Cell Phenotype in PDA Is Influenced by Diverse Inflammatory and Microbial Signals

Because CCR2 recruits innate T cells to the PDA TME (Fig. 1K; ref. 5), we postulated that CCR2 signaling also modulates iαβT cellular phenotype *in situ*. Accordingly, intratumoral iαβT-cell expression of T-bet and CD44 was reduced in CCR2$^{-/-}$ hosts, expression of ICOS, CTLA4, and TIM3 was upregulated, and cytokine expression was not altered (Supplementary Fig. S4a). Because we previously reported that Dectin-1 can regulate cytokine secretion in unconventional T cells (9), we postulated that, unlike CCR2, Dectin-1 signaling may govern iαβT-cell cytokine profile. PDA-infiltrating iαβTs in Dectin-1$^{-/-}$ mice expressed reduced IL17 and IFNγ, whereas TNFα expression was unchanged (Supplementary Fig. S4b). Accordingly, ligating Dectin-1 upregulated IFNγ and IL17 in naïve splenic iαβTs (Supplementary Fig. S4c). Collectively, these data suggest that CCR2 and Dectin-1 signals influence distinct aspects of iαβT-cell programming in PDA.

We recently reported that the host microbiome in PDA exerts suppressive influences on intratumoral CD4$^+$ and CD8$^+$ T-cell differentiation (10). We therefore postulated that the PDA microbiome has similar tolerogenic effects on iαβTs. To test this, we ablated the microbiome in PDA-bearing mice using an established oral antibiotic regimen (Supplementary Fig. S4d; ref. 11). Consistent with our hypothesis, microbial ablation activated iαβTs, increasing their expression of T-bet, CD44, LFA-1, ICOS, IL17, IFNγ, and TNFα (Supplementary Fig. S4e). Mechanistically, we reported that the microbiome directs immune suppression in PDA via TLR4 signaling (10, 12). Interestingly, we found that iαβTs upregulate TLR4 expression in PDA (Supplementary Fig. S4f). Consistent with our analysis of PDA-infiltrating CD4$^+$ and CD8$^+$ T cells (10), TLR4 ligation mitigated iαβT-cell activation (Supplementary Fig. S4g).

iαβTs Protect against PDA and Induce Immunogenic CD4$^+$ and CD8$^+$ T-cell Activation in Mouse and Human Models

To determine the influence of iαβTs on pancreatic oncogenesis, we adoptively transferred iαβTs to mice coincident with subcutaneous tumor challenge. iαβT-cell administration mitigated pancreatic tumor growth (Fig. 3A). iαβT-cell transfer resulted in intratumoral CD8$^+$ T-cell activation (Fig. 3B). Similarly, intrapancreatic iαβT cellular transfer with orthotopically implanted KPC tumor cells protected against tumor growth (Fig. 3C) and again activated CD4$^+$ and CD8$^+$ T cells in the TME, inducing higher expression of CD44, ICOS, and TNFα (Fig. 3D–F). To determine whether iαβTs are suitable agents for cellular therapy, we serially administered iαβTs intravenously to mice bearing established orthotopic PDA tumors. iαβT administration protected against tumor growth and immunogenically reprogrammed the adaptive TME (Fig. 3G–J). Furthermore, analysis of tumors treated with iαβTs by single-cell RNA-seq suggested a marked CD4$^+$ and CD8$^+$ T-cell expansion compared with controls. Specifically, conventional T-cell populations increased from 3% to 20% of leukocytes with iαβT-cell treatment (Fig. 3K and L). Other lymphocyte subsets were also expanded. Consistent with our flow cytometry data, conventional T cells

Figure 2. iαβTs infiltrating PDA are phenotypically distinct. WT mice bearing orthotopic KPC tumors were sacrificed on day 21. **A–G,** Splenic and PDA-infiltrating iαβTs were tested for expression of JAML (**A**), CD107a (**B**), CTLA4 (**C**), TIM3 (**D**), PD-1 (**E**), CD39 (**F**), and CD40L, LAG3, CD73, ICOS, and Dectin-1 (**G**). **H,** Splenic and PDA-infiltrating iαβTs were tested for expression of CD62L. **I,** TCR sequencing of splenic iαβTs and PDA-infiltrating iαβTs, CD4$^+$ and CD8$^+$ T cells was performed in triplicate and assessed for overlapping clones between populations. **J,** Splenic and PDA-infiltrating iαβTs, CD4$^+$ T cells, and CD8$^+$ T cells were tested for expression of T-bet. **K,** Splenic and orthotopic PDA-infiltrating iαβTs were tested for coexpression of IFNγ and IL17A. **L,** PDA-infiltrating CD3$^+$IL17$^+$ cells were gated and tested for the frequency of CD4$^+$ T cells, CD8$^+$ T cells, NKT cells, γδT cells, and iαβTs. **M,** Splenic and PDA-infiltrating iαβTs were cultured *in vitro* for 24 hours and cell culture supernatant was harvested and assayed for IL17, IFNγ, and IL10 ($n = 5$/group). Flow cytometry experiments were repeated more than 4 times with similar result. $n = 5$ mice for each replicate experiment; *, $P < 0.05$; **, $P < 0.01$; ***, $P < 0.001$; ****, $P < 0.0001$.

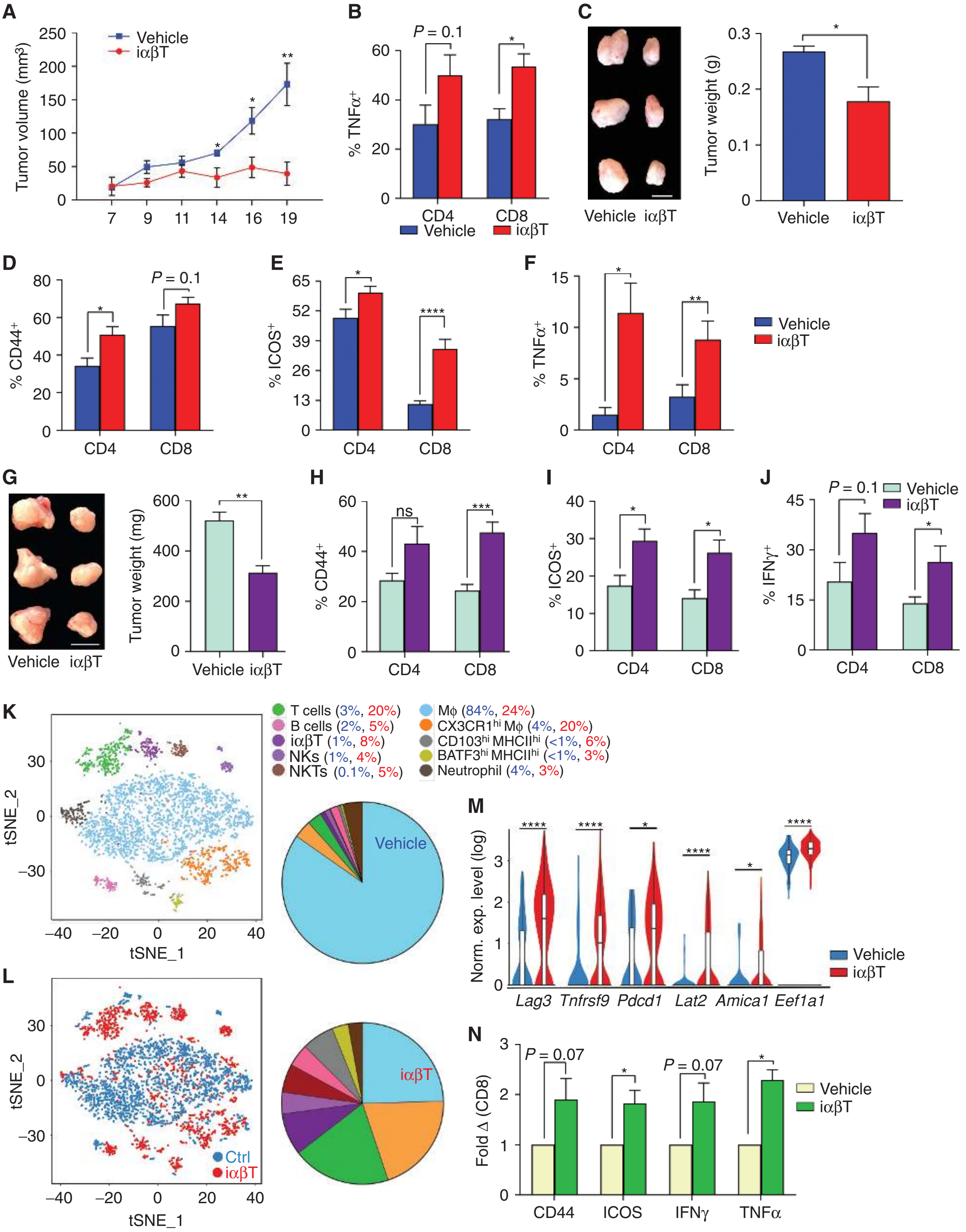
A
Tumor volume (mm3)
250
200
150
100
50
0
7 9 11 14 16 19
Vehicle
iαβT
*
*
**
B
% TNFα+
P = 0.1
*
60
40
20
0
CD4 CD8
Vehicle iαβT
C
Vehicle iαβT
Tumor weight (g)
0.3
0.2
0.1
0
*
Vehicle iαβT
D
% CD44+
80 60 40 20 0
*
P = 0.1
CD4 CD8
E
% ICOS+
65 52 39 26 13 0
*
****
CD4 CD8
F
% TNFα+
15 10 5 0
*
**
CD4 CD8
Vehicle
iαβT
G
Vehicle iαβT
Tumor weight (mg)
600 400 200 0
**
Vehicle iαβT
H
% CD44+
60 40 20 0
ns
***
CD4 CD8
I
% ICOS+
40 30 20 10 0
*
*
CD4 CD8
J
% IFNγ+
45 30 15 0
P = 0.1
*
Vehicle
iαβT
CD4 CD8
K
tSNE_2
30 0 −30
−40 −20 0 20 40
tSNE_1
T cells (3%, 20%)
B cells (2%, 5%)
iαβT (1%, 8%)
NKs (1%, 4%)
NKTs (0.1%, 5%)
Mϕ (84%, 24%)
CX3CR1hi Mϕ (4%, 20%)
CD103hi MHCIIhi (<1%, 6%)
BATF3hi MHCIIhi (<1%, 3%)
Neutrophil (4%, 3%)
Vehicle
L
tSNE_2
30 0 −30
−40 −20 0 20 40
tSNE_1
Ctrl
iαβT
iαβT
M
Norm. exp. level (log)
3 2 1 0
****
****
*
****
*
****
Lag3 Tnfrsf9 Pdcd1 Lat2 Amica1 Eef1a1
Vehicle
iαβT
N
Fold Δ (CD8)
3 2 1 0
P = 0.07
*
P = 0.07
*
CD44 ICOS IFNγ TNFα
Vehicle
iαβT

in tumors of iαβT cell–treated mice expressed higher activation markers (*Lag3, Tnfrsf9, Pdcd1,* and *Lat2*), indicators of cytotoxicity (*Amica1*), and Th1-related transcription factors (*Eef1a1*; Fig. 3m; Supplementary Fig. S5a).

To determine whether iαβTs have the capacity to immunogenically reprogram adaptive immunity in human disease, we generated patient-derived organotypic tumor spheroids (PDOTS) from freshly harvested human tumors using a microfluidic-based system that we recently described (13). We selectively added FACS-sorted autologous iαβTs or vehicle to the PDOTS and analyzed the system at 3 days. Consistent with our murine data, iαβTs induced marked conventional T-cell activation in the human PDOTS system (Fig. 3N; Supplementary Fig. S5b).

PDA-Infiltrating iαβTs Induce Effector T Cell–Dependent Tumor Protection, but Paradoxically Suppress Conventional T Cells *In Vitro*

In addition to expressing high levels of the cytotoxicity marker CD107a (Fig. 2B), PDA-associated iαβTs also upregulate FasL, Perforin, and Granzyme B (Fig. 4A). We therefore postulated that iαβTs may be directly cytotoxic to PDA tumor cells. However, iαβTs did not mitigate tumor cell proliferation, induce tumor cell lysis, or promote apoptosis (Fig. 4B–D). Because iαβT cellular transfer enhanced T-cell immunity *in situ*, we speculated that iαβTs mediate tumor protection by directly activating $CD4^+$ and $CD8^+$ T cells in the PDA microenvironment. Accordingly, whereas $CD4^+$/$CD8^+$ T-cell depletion did not accelerate tumor progression in control mice as we previously reported (5, 10), $CD4^+$/$CD8^+$ T-cell depletion abrogated the tumor protection associated with iαβT transfer (Fig. 4E). We therefore used *in vitro* modeling to determine whether iαβTs directly enhance αβT cell immunogenicity. Belying our *in vivo* data, we found that PDA-infiltrating iαβTs were highly inhibitory to $CD4^+$ and $CD8^+$ T-cell activation *in vitro* and prevented their upregulation of IFNγ, TNFα, T-bet, CD69, and CD44 in response to CD3/CD28 coligation (Figs. 4F–I; Supplementary Fig. S5C). iαβTs similarly mitigated polyclonal T-cell secretion of IFNγ, TNFα, and IL2 in cell culture supernatant (Fig. 4J). Further, iαβTs promoted upregulation of FOXP3 expression in $CD4^+$ T cells (Fig. 4K). The inhibitory effects of iαβTs on conventional T cells were independent of TGFβ secretion (Supplementary Fig. S5d–f). We previously reported that γδT cells can inhibit $CD4^+$ and $CD8^+$ T-cell activation in cancer via the PD-L1–PD-1 axis (5). Therefore, we postulated that iαβTs, which upregulate PD-L1 in PDA (Fig. 4L), suppress effector T cells through PD-L1–PD-1 interactions. PD-L1 blockade partially reversed the inhibitory effects of PDA-infiltrating iαβTs on effector T-cell activation (Fig. 4M and N).

PDA-Associated iαβTs Promote Immunogenic Macrophage Polarization via CCR5 Activation

We previously showed that macrophage programming governs the balance between T-cell tolerance and immunogenicity in PDA (5, 14). Therefore, we postulated that iαβTs may indirectly augment intratumoral adaptive immunity by inducing immunogenic macrophage polarization, which in turn reprograms effector T-cell populations. Accordingly, iαβTs directly upregulated macrophage expression of MHCII, CD38, IL6, and TNFα in coculture experiments (Fig. 5A). iαβTs also promoted increased CD86 and IFNγ expression in macrophages and downregulated CD206 and IL10 (Fig. 5B and C). *In vivo* iαβT-cell transfer in PDA also induced higher MHCII, iNOS, TNFα, IFNγ, and IL12 expression in TAMs, whereas CD206 and IL10 expression was reduced (Fig. 5D). iαβT-cell transfer also significantly increased STAT1 signaling in TAMs, which is linked to M1-like macrophage polarization (Fig. 5E). Further, our single-cell RNA-seq data indicated a marked contraction of *F480*^{hi} macrophages in tumors after serial iαβT-cell transfer. Specifically, macrophages represented 84% of leukocytes in control tumors compared with only 24% in iαβT cell–treated mice (Fig. 3L and M). Moreover, consistent with our flow cytometry data, iαβT-cell transfer resulted in upregulation of genes related to antigen presentation (e.g., H2-family genes, *Cd74, B2m*), T-cell chemoattraction (*Ccl5, Cxcl9, Cxcl10*), IFN signaling (*Stat1, Ifnar1, Ifngr1, Irf5, Irf7, Irf8*), and M1 polarization (*Tnf, Ccl9, Il6ra, Ccr5*) on macrophages, whereas M2-associated transcription factors were downregulated (*Stat6, Socs3, Il1b*; Supplementary Fig. S6a–e). Ingenuity pathway analysis of upstream regulators indicated that *Stat1*, *Ifnγ*, and *Tnfα* signaling was significantly activated in TAM-infiltrating tumors of iαβT cell–treated mice relative to controls (Supplementary Fig. S6f–h). Further, gene set enrichment analysis (GSEA) indicated significant enrichment of "KEGG_Antigen processing and presentation" and "KEGG_Chemokine signaling pathway" in macrophages of iαβT cell–treated tumors (Supplementary Fig. S6i and j).

Figure 3. iαβTs protect against PDA and enhance intratumoral T-cell immunity. **A,** WT mice were administered KPC tumor cells subcutaneously, either alone or admixed with iαβTs. Tumor growth was serially measured ($n = 5$/group). **B,** WT mice were administered KPC tumor cells subcutaneously, either alone or admixed with PDA-infiltrating iαβTs. On day 21, tumor-infiltrating $CD8^+$ T cells were analyzed for expression of TNFα ($n = 5$/group). **C–F,** WT mice were orthotopically administered KPC tumor cells, either alone or admixed with iαβTs. Tumors were harvested on day 21. **C,** Representative pictures of tumors and quantitative analysis of tumor weight are shown. Scale bar, 5 mm. **D–F,** PDA-infiltrating $CD4^+$ and $CD8^+$ T cells were analyzed for expression of CD44 (**D**), ICOS (**E**), and TNFα (**F**; $n = 5$/group). Each mouse experiment was repeated more than 3 times. **G–J,** Mice with established orthotopic KPC tumor were serially transferred intravenously twice weekly with iαβTs or vehicle beginning on day 5 ($n = 5$). Mice were sacrificed at day 21 after tumor implantation. **G,** Representative pictures of tumors and quantitative analysis of tumor weight are shown. Scale bar, 5 mm. **H–J,** PDA-infiltrating $CD4^+$ and $CD8^+$ T cells were analyzed for expression of CD44 (**H**), ICOS (**I**), and IFNγ (**J**). Subcutaneous and orthotopic tumor experiments were each repeated at least 4 times. **K–M,** Mice with established orthotopic KPC tumors were serially transferred intravenously twice weekly with iαβTs or vehicle beginning on day 5. Mice were sacrificed at day 21 and single-cell RNA-seq performed on FACS-purified $CD45^+$ tumor-infiltrating leukocytes. **K,** The distribution of cellular clusters was determined using the t-SNE algorithm. Each cluster is identified by a distinct color. **L,** A t-SNE plot overlay of tumor-infiltrating leukocytes in tumors of mice treated with iαβTs (red) vs. vehicle (blue) is shown. Percent cellular abundance in each cluster is depicted in pie charts and specified in the accompanying legend. **M,** Violin plots comparing normalized log expression of select genes in the T-cell cluster for both treatment groups are shown. **N,** PDOTS derived from resected human tumors were treated with autologous iαβTs or vehicle. At 72 hours, $CD8^+$ T cells were analyzed for expression of CD44, ICOS, IFNγ, and TNFα. Data are indicated as fold change in the iαβT cell–treated group compared with vehicle treated. $n = 5$ patients; *, $P < 0.05$; **, $P < 0.01$; ***, $P < 0.001$; ****, $P < 0.0001$.

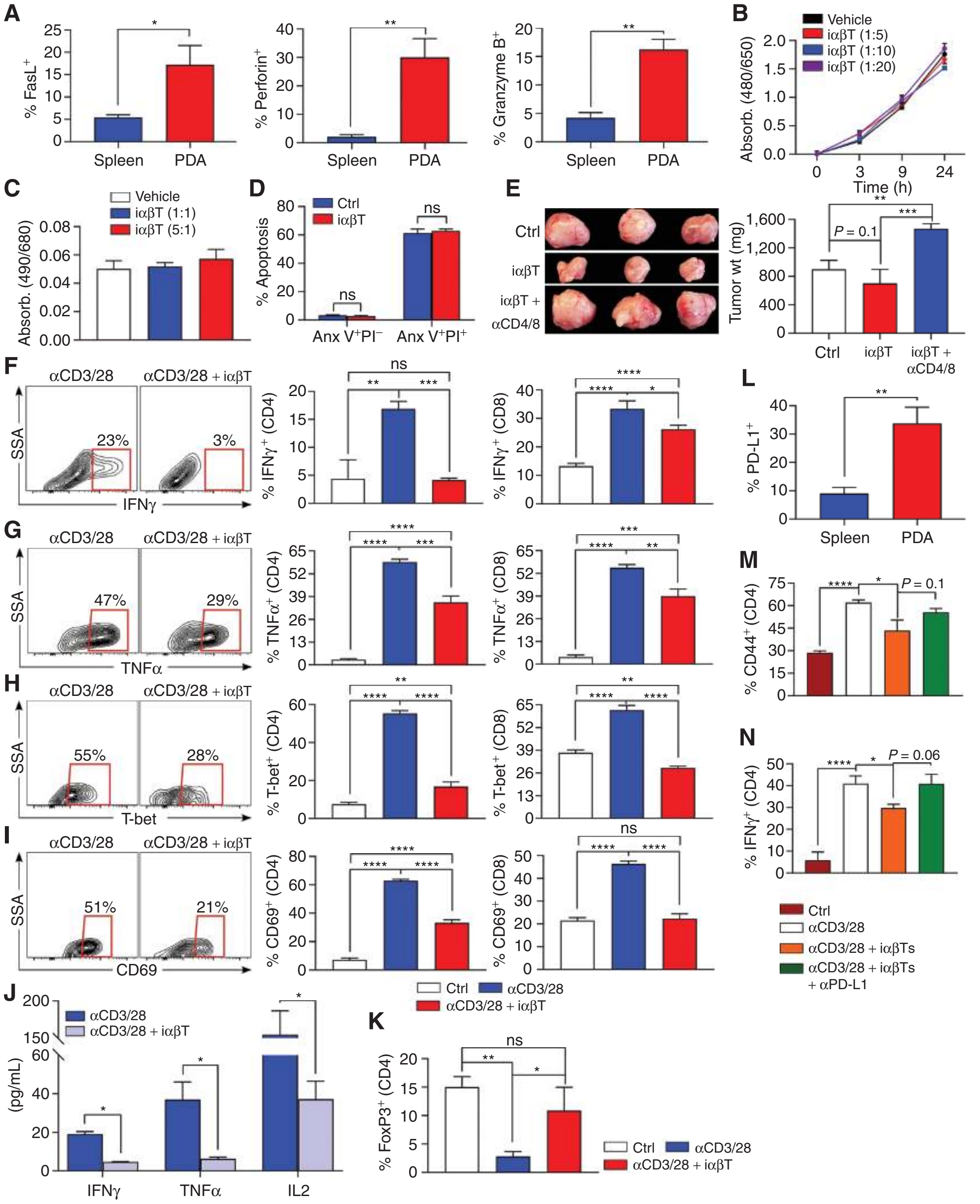

Figure 4. iαβTs induce T cell–dependent tumor immunity but are directly suppressive to conventional T cells. **A,** WT mice bearing orthotopic KPC tumors were sacrificed on day 21. Splenic and PDA-infiltrating iαβTs were tested for expression of FasL, Perforin, and Granzyme B ($n = 5$ mice). **B** and **C,** iαβTs were harvested by FACS from orthotopic PDA tumors and cultured in various ratios with KPC tumor cells. **B,** Proliferation of KPC tumors cells was tested using the XTT assay. **C,** Cytotoxicity against KPC tumor cells was determined in an LDH release assay. **D,** iαβTs were harvested by FACS from orthotopic PDA tumors and cultured in 1:1 ratio with KPC tumor cells. KPC tumor cell apoptosis was determined by costaining for Annexin V and PI. **E,** WT mice were orthotopically administered KPC tumor cells admixed with iαβTs. Cohorts were either serially depleted of both $CD4^+$ and $CD8^+$ T cells or administered isotype control before sacrifice on day 21. Representative images and quantitative analysis of tumor weights are shown ($n = 5$/group). This experiment was repeated twice. **F–I,** Polyclonal splenic $CD4^+$ or $CD8^+$ T cells were cultured without stimulation, stimulated by CD3/CD28 coligation, or stimulated by CD3/CD28 coligation in coculture with iαβTs. $CD4^+$ and $CD8^+$ T-cell activation was determined at 72 hours by their expression of IFNγ (**F**), TNFα (**G**), T-bet (**H**), and CD69 (**I**). Representative contour plots and quantitative data are shown. **J,** Polyclonal splenic $CD3^+$ T cells were stimulated by CD3/CD28 coligation, either alone or in coculture with iαβTs. Cell culture supernatant was tested for expression of IFNγ, TNFα, and IL2 at 72 hours. **K,** Polyclonal splenic $CD4^+$ T cells were cultured without stimulation, stimulated by CD3/CD28 coligation, or stimulated by CD3/CD28 coligation in coculture with iαβTs. $CD4^+$ T cells were tested for expression of FOXP3 at 72 hours. **L,** Spleen and PDA-infiltrating iαβTs were tested for expression of PD-L1 by flow cytometry. **M** and **N,** Polyclonal splenic $CD4^+$ T cells from PD-$L1^{-/-}$ mice were cultured without stimulation, stimulated by CD3/CD28 coligation, or stimulated by CD3/CD28 coligation in coculture with WT iαβTs, either alone or with an αPD-L1–neutralizing mAb. $CD4^+$ T cells were tested for expression of CD44 (**M**) and IFNγ (**N**) at 72 hours. Experiments were performed in replicates of 5 and repeated at least 4 times. *, $P < 0.05$; **, $P < 0.01$; ***, $P < 0.001$; ****, $P < 0.0001$.

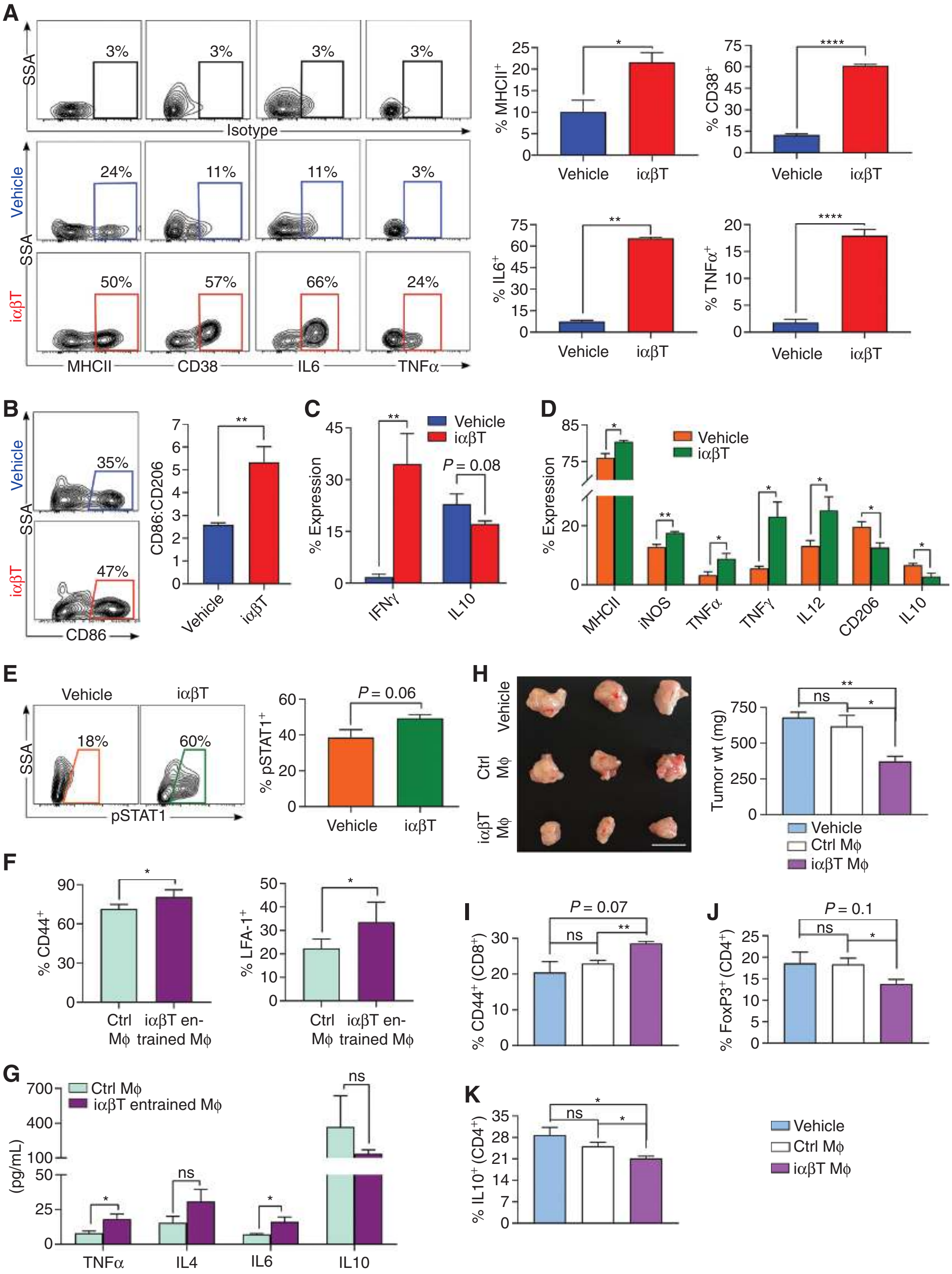

Figure 5. iαβTs induce immunogenic reprogramming of macrophages. **A–C,** Splenic macrophages were cultured alone or cocultured with iαβTs for 24 hours. Macrophages were then harvested and tested for expression of MHC II, CD38, IL6, and TNFα (**A**), CD86 and CD206 (**B**), IFNγ and IL10 (**C**). Select contour plots and quantitative data are shown. This experiment was repeated 5 times. **D** and **E,** KPC tumor-bearing mice were adoptively transferred with iαβTs. Tumors were harvested on day 21 and TAMs were analyzed for expression of MHCII, iNOS, TNFα, IFNγ, IL12, CD206, and IL10 (**D**), and pSTAT1 (**E**). This experiment was repeated twice ($n = 5$/group). **F** and **G,** iαβT cell–entrained splenic macrophages and control splenic macrophages were pulsed with Ova$_{323-339}$ peptide and used to stimulated Ova-restricted CD4$^+$ T cells. T-cell activation was determined at 96 hours by expression of (**F**) CD44 and LFA-1. **G,** Cell culture supernatant was harvested and tested for expression of TNFα, IL4, IL6, and IL10. *In vitro* experiments were performed in replicates of 5 and repeated 3 times. **H–K,** Cohorts of WT mice were administered orthotopic KPC tumor either alone, admixed with control macrophages or macrophages that had been cocultured with iαβTs. Pancreatic tumors were harvested on day 21 ($n = 5$/group). **H,** Tumor weights were recorded. Scale bar, 5 mm. **I,** Tumor-infiltrating CD8$^+$ T cells were analyzed for expression of CD44. Tumor-infiltrating CD4$^+$ T cells were analyzed for expression of FOXP3 (**J**) and IL10 (**K**). This experiment was repeated twice. *, $P < 0.05$; **, $P < 0.01$; ***, $P < 0.001$; ****, $P < 0.0001$.

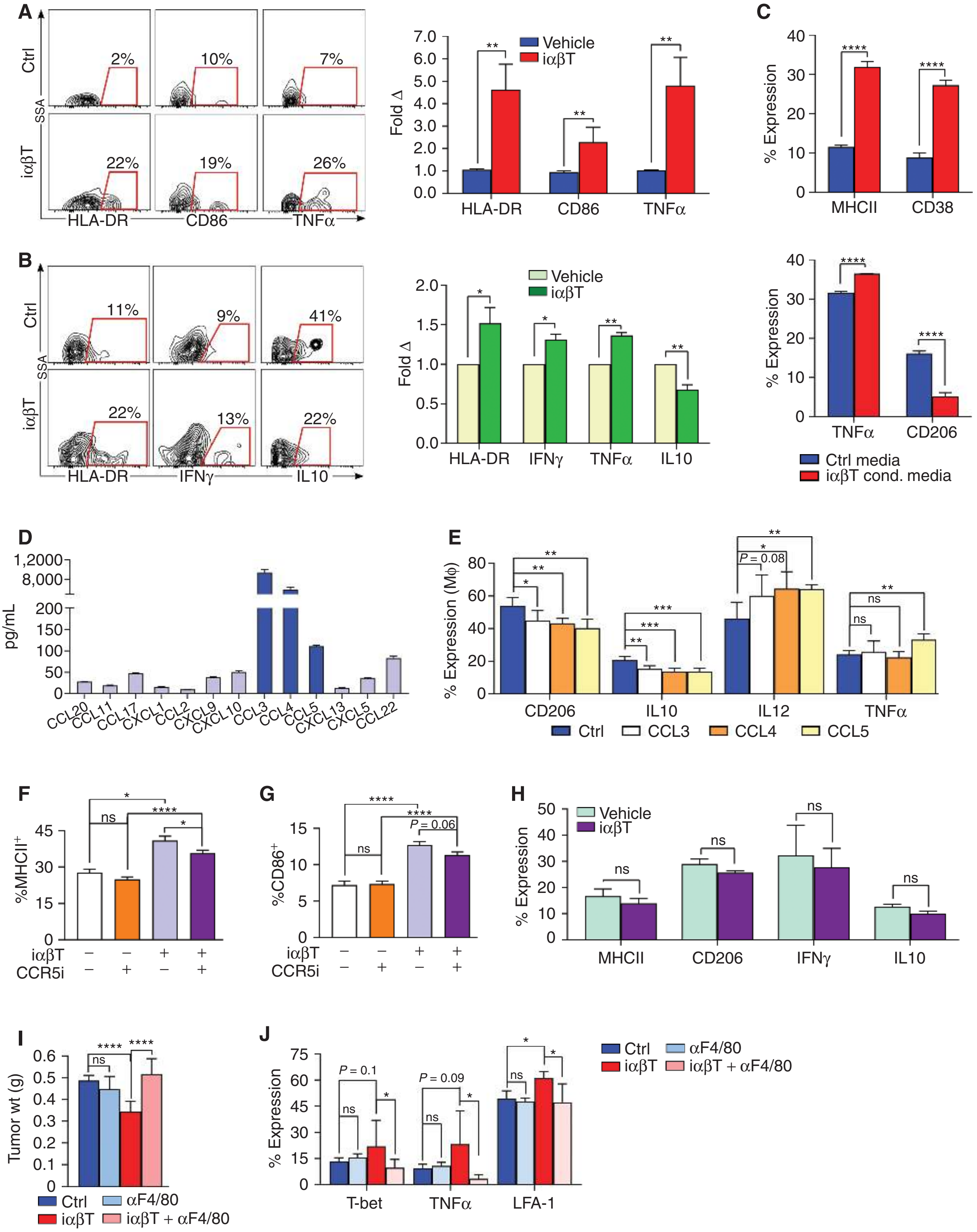
A
Ctrl
iαβT
SSA
2%
10%
7%
22%
19%
26%
HLA-DR
CD86
TNFα
Fold Δ
7.0
6.0
5.0
4.0
3.0
2.0
1.0
0.0
Vehicle
iαβT
**
**
**
HLA-DR
CD86
TNFα
C
% Expression
40
30
20
10
0
****
****
MHCII
CD38
B
Ctrl
iαβT
SSA
11%
9%
41%
22%
13%
22%
HLA-DR
IFNγ
IL10
Fold Δ
2.0
1.5
1.0
0.5
0.0
Vehicle
iαβT
*
*
**
**
HLA-DR
IFNγ
TNFα
IL10
% Expression
40
30
20
10
0
****
****
TNFα
CD206
Ctrl media
iαβT cond. media
D
pg/mL
1,2000
8,000
200
150
100
50
0
CCL20
CCL11
CCL17
CXCL1
CCL2
CXCL9
CXCL10
CCL3
CCL4
CCL5
CXCL13
CXCL5
CCL22
E
% Expression (MΦ)
80
60
40
20
0
*
**
**
**
***
***
**
*
P = 0.08
ns
ns
**
CD206
IL10
IL12
TNFα
Ctrl
CCL3
CCL4
CCL5
F
%MHCII⁺
45
30
15
0
*
ns
****
*
iαβT
CCR5i
− − + +
− + − +
G
%CD86⁺
15
10
5
0
****
****
ns
P = 0.06
iαβT
CCR5i
− − + +
− + − +
H
% Expression
50
40
30
20
10
0
Vehicle
iαβT
ns
ns
ns
ns
MHCII
CD206
IFNγ
IL10
I
Tumor wt (g)
0.6
0.5
0.4
0.3
0.2
0.1
0
****
****
ns
Ctrl
αF4/80
iαβT
iαβT + αF4/80
J
% Expression
75
60
45
30
15
0
P = 0.1
ns
*
P = 0.09
ns
*
*
ns
*
T-bet
TNFα
LFA-1
Ctrl
αF4/80
iαβT
iαβT + αF4/80

Finally, we noted the expansion of a distinct *Cx3cr1*^{hi}*F480*^{hi} macrophage population in the TME of iαβT cell–treated mice (Fig. 3L and M). This population upregulated *Ccl5,* but did not exhibit upregulation of the other genes and pathways related to antigen presentation and proinflammatory signaling observed in the broader macrophage population (Supplementary Fig. S6K). Collectively, these data show that iαβTs induce profound immunogenic macrophage programming in PDA.

We postulated that iαβTs secondarily augment adaptive T-cell immunity *in situ* via their immunogenic influence on macrophage differentiation. To test this, antigen-pulsed macrophages entrained by coculture with iαβTs were used to stimulate antigen-restricted CD4$^+$ T cells. Consistent with our hypothesis, iαβT-entrained macrophages were more efficient than controls at antigen presentation based on T-cell expression of activation markers and secreted cytokines (Fig. 5F and G). Moreover, *in vivo* adoptive transfer of macrophages entrained by iαβT coculture was markedly protective against PDA, whereas transfer of control macrophages was not (Fig. 5H). Adoptive transfer of iαβT-entrained macrophages also activated intratumoral conventional T cells and reduced Treg differentiation *in situ* (Fig. 5I–K). Collectively, these data suggest that iαβTs can induce macrophage-mediated adaptive antitumor immunity in PDA. To determine whether iαβTs also activate macrophages in human systems, we cocultured FACS-sorted iαβTs with human PBMC-derived macrophages. Consistent with our murine data, iαβTs activated human macrophages (Fig. 6A). Furthermore, autologous treatment of organotypic 3-D models of human PDA with iαβTs similarly resulted in marked activation of TAMs (Fig. 6B).

Mechanistically, we postulated that iαβTs secrete specific inflammatory mediators that may drive immunogenic macrophage programming. To test this, we cultured naïve splenic macrophages with iαβT cell–conditioned media or control media. iαβT-conditioned media upregulated MHC II, CD38, and TNFα in macrophages and downregulated CD206, suggesting that iαβT-derived secreted factors are sufficient to induce an activated macrophage phenotype (Fig. 6C). To determine the mechanism through which iαβTs regulate macrophage polarization, we performed unbiased analysis of inflammatory mediators secreted by iαβTs. We found that iαβTs produced markedly high levels of CCL3, CCL4, and CCL5, each of which ligate CCR5 (Fig. 6D; ref. 15). Consistent with our hypothesis, treatment of macrophages with rCCL3, rCCL4, and rCCL5 induced M1-like differentiation (Fig. 6E). Further, CCR5 inhibition mitigated immunogenic macrophage polarization induced by iαβTs (Fig. 6F and G). CCR5$^{-/-}$ macrophages similarly failed to become activated in coculture with iαβTs (Fig. 6H). Collectively, these data suggest that iαβTs program macrophages by secretion of factors that engage the CCR5 axis. Corroboratively, *in vivo* depletion of macrophages abrogated the tumor protection and effector T-cell activation observed with iαβT-cell adoptive transfer (Fig. 6I and J).

DISCUSSION

We show that TCRαβ$^+$CD4$^-$CD8$^-$NK1.1$^-$ represent ~10% of T cells in the mouse and human PDA TME. These cells differ from innate lymphoid cells by expression of the CD3–TCR complex and are distinguished from NKT cells by the absence of obligate marker expression on transcriptomic and flow-cytometric analyses. Interestingly, our iαβTs share some phenotypic features with mucosal associated invariant T (MAIT) cells, a subset of CD3$^+$ T cells that can express CD4 and CD8, but are classically CD4$^-$CD8$^-$. MAIT cells predominate in the gut, where they defend against microbial infection, but have been described in the blood, liver, and lungs (16). Given that PDA-infiltrating iαβTs and MAIT cells both exhibit high expression of cytokines, including IL17 and IFNγ, as well as production of cytolytic molecules such as Perforin and Granzyme B, we probed the antigen specificity of PDA-infiltrating iαβT and gut-derived MAIT cells (17). The MHC class I–like protein MR1 is responsible for presenting bacterially produced vitamin B metabolites to MAIT cells. In turn, recognition of antigen results in MAIT cell stimulation and secretion of proinflammatory cytokines (18). However, we found that only ~10% of iαβTs in PDA recognize a murine MR1-specific tetramer, as compared with ~40% of CD3$^+$CD4$^-$CD8$^-$ cells in the gut. CD4$^+$ and CD8$^+$ T cells in PDA expressed similar levels of the MR1-specific tetramer compared with iαβT cells. Thus, although the cytokine profiles remain similar, we are averse to define our population as MAIT cells and prefer their more general description as iαβTs. We maintain the possibility that iαβTs in PDA encompass a diversity of phenotypes, as do most broadly described T-cell populations, but the precise cellular ontogeny is beyond the scope of our work. Rather, our investigations focus on the impact of these cells in interfacing with other innate and adaptive immune subsets, as novel targets of immunotherapy, and their role in combating oncogenic progression.

Figure 6. iαβTs induce immunogenic macrophage programming via CCR5 activation. **A,** iαβTs were FACS sorted from three healthy volunteers and cocultured with autologous naïve PBMC-derived macrophages. At 24 hours, macrophage expression of HLA-DR, CD86, and TNFα was determined by flow cytometry. Experiments for each individual were performed in triplicate. Representative contour plots are shown, and quantitative data are presented as fold change in expression compared with macrophages cultured alone. **B,** Human PDOTS were treated with autologous iαβTs or vehicle. TAMs were tested for expression of HLA-DR, IFNγ, TNFα, and IL10. Representative contour plots are shown, and quantitative data are indicated as fold change in expression compared with vehicle treatment ($n = 5$ patients). **C,** Naïve macrophages were cultured with iαβT cell–conditioned media or control media. After 24 hours, macrophage expression of MHCII, CD38, TNFα, and CD206 was determined by flow cytometry. This experiment was repeated 3 times. **D,** iαβTs were FACS sorted from orthotopic PDA tumors and cultured for 24 hours. Cell culture supernatant was analyzed in a chemokine array. This experiment was repeated twice ($n = 5$). **E,** WT bone marrow–derived macrophages were treated with rCCL3, rCCL4, rCCL5, or vehicle and assessed at 24 hours. **F** and **G,** WT-derived macrophages were cultured alone or cocultured with PDA-infiltrating iαβTs for 24 hours. A CCR5 small-molecule inhibitor (CCR5i) or vehicle was added to select wells. Macrophage expression of MHC II (**F**) and CD86 (**G**). This experiment was repeated 3 times ($n = 5$/group). **H,** CCR5$^{-/-}$ macrophages were cultured with PDA-infiltrating iαβTs for 24 hours. Macrophage expression of MHC II, CD206, IFNγ, and IL10 was determined. This experiment was repeated 4 times in replicates of 5. **I** and **J,** Orthotopic PDA tumors were harvested from control WT mice or WT mice treated with αF4/80, iαβT-cell transfer, or αF4/80 plus iαβT-cell transfer. Tumor weights were measured (**I**) and CD8$^+$ T-cell activation was determined by expression of T-bet, TNFα, and LFA-1 (**J**). $n = 7$/group. *, $P < 0.05$; **, $P < 0.01$; ***, $P < 0.001$; ****, $P < 0.0001$.

The PDA microenvironment is regulated by diverse cellular and biochemical inflammatory signals that modulate tumor growth. However, the cross-talk between cellular subsets in the inflammatory TME remains incompletely understood. The importance of unconventional T-cell subsets in this immune interplay is becoming increasingly recognized in both hematologic and solid organ malignancies. For example, in PDA we showed that γδT cells cripple conventional $CD4^+$ and $CD8^+$ T-cell immunogenicity via upregulation of PD-L1 and Galectin-9 (5). By contrast, NKT cells exhibit protective effects in preinvasive models of PDA via monocytic cross-talk (6). Consistent with the role of NKT cells as first responders in inflammation (19, 20), we found that NKT cell levels steadily declined in PDA as tumors progressed, whereas iαβTs sharply increased in the TME over the course of disease progression. This latter observation is consistent with high levels of CCL2 in mature PDA tumors (21), as we discovered that iαβTs are recruited to the TME via CCR2 signaling.

We found that iαβTs are distinctly proinflammatory in PDA, promiscuously expressing high costimulatory (ICOS and CD40L) and checkpoint (CTLA4, PD-1, TIM3, and LAG3) receptors and coexpressing both Th1 and Th17 families of fate-determining transcription factors (T-bet and RORγt) and cytokines (IFNγ and IL17). However, in contrast to the tolerogenic role of iαβTs in the context of organ transplantation (19), PDA-infiltrating iαβTs minimally express FOXP3 and IL10, consistent with their more immunogenic function. Interestingly, the tumor-protective effects of iαβTs belie the fact that these cells are the highest producers of IL17 in PDA, a cytokine that has been shown to have directly proliferative effects on tumor cells (20). Though we observed that iαβTs possess a cytotoxic phenotype in PDA (expression of perforins, granzymes, and FasL), they were incapable of directly inhibiting tumor proliferation or inducing tumor cell death *in vitro*. This contrasts with findings in melanoma and lymphoma where iαβTs exhibit potent tumor-specific cytotoxicity (22, 23). This observation could in theory be due to the paucity of tumor-associated antigens (TAA) and neoantigens in PDA relative to other cancers and the consequent limitation of MHCI-dependent killing. However, we observed that iαβTs in PDA do not recognize tumor antigen; therefore, their lack of directly tumoricidal properties is unlikely solely due to the scarcity of TAA.

We found that iαβTs delimit PDA progression by shaping the innate and adaptive immunologic landscape. Specifically, iαβTs promote macrophage reprogramming to a distinctly immunogenic phenotype, which in turn enhances effector $CD4^+$ and $CD8^+$ T-cell function. Several studies have shown that TAMs drive tumor progression in PDA by possessing potent immunosuppressive properties (24–26). Interestingly, we show that treatment with iαβTs not only results in the global contraction of TAMs in the PDA TME, but also confers significant proinflammatory phenotypic changes to the remaining macrophages, leading to the expansion of effector T-cell populations. We also found that deletion of TAMs abrogated the tumor protection and enhancement in adaptive immunity associated with iαβT-cell transfer. Programs upregulated in TAMs by treatment with iαβTs included antigen presentation, T-cell chemoattraction, and IFN, TNF, and STAT1 signaling. In this way, iαβTs may shift the balance toward antitumor immunity by dually abrogating immune suppression and promoting increased antigen presentation capacity to effector T cells and their activation (Supplementary Fig. S7). We found that the iαβT cell–macrophage cross-talk was linked to the high levels of CCR5 ligands secreted by iαβTs. Moreover, considering the central role of TAMs in regulating the adaptive immune program and the protective tumor immunity associated with iαβT cellular transfer, our data suggest that iαβTs may be attractive vehicles for cell therapy in PDA.

This work also highlights paradoxical effects regarding the influence of iαβTs on $CD4^+$ and $CD8^+$ T cells. We show that iαβTs directly inhibit $CD4^+$ and $CD8^+$ T cells *in vitro* in coculture experiments via the PD-L1–PD-1 axis. This parallels the suppressive effects of γδT cells in PDA (5). Conversely, the broader *in vivo* effect of iαβTs is a downstream immunogenic activation of effector T cells via macrophage activation. These findings are consistent with previous work suggesting that TAM programming is the dominant driver of the adaptive immune landscape in PDA (14, 24). This functional hierarchy is even more plausible considering that the iαβT-mediated suppressive effect on effector T cells requires direct cell contact via PD-L1–PD1 interaction, whereas macrophage activation can occur remotely via secretion of CCL3, CCL4, and CCL5 (CCR5 ligands). The contact-dependent inhibitory effects of iαβTs on effector T cells, activating effects (including PD-1 upregulation) observed after iαβT-cell transfer on effector T cells, and the observed activation of iαβTs in response to αPD-L1 therapy *in vivo* suggest that immunotherapy targeting the PD-L1–PD-1 axis could synergistically accentuate the tumor-protective and immunologic benefits of iαβT cell–directed therapies.

The signals that drive the distinctive phenotype of iαβTs in PDA are diverse and modifiable and collectively account for their complex features. Signaling via Dectin-1, a pattern recognition receptor capable of binding Galectin-9 and fungal wall β-glucans, promoted IFNγ and IL17 production in iαβTs, but did not appreciably modulate iαβT surface phenotype. By contrast, CCR2 signaling activated iαβT cell–surface phenotype and upregulated expression of costimulatory and checkpoint receptors, but did not alter cytokine production. The PDA-associated microbiome and LPS have broadly suppressive effects on iαβTs, reducing both cytokine and surface activation marker expression. Therefore, tailored approaches can be used to modulate iαβT cell phenotype *in situ* or *ex vivo* to optimize phenotypic outcomes. Finally, the use of iαβTs as an adoptive cell therapy into human organotypic PDOT systems of pancreatic cancer is the first application of its kind. The ability for iαβTs to induce significant immunogenic activation in these 3-D human systems illustrates their potential as a novel cell therapy. In aggregate, our work suggests that iαβT-cell cross-talk serves to connect innate and adaptive immunity in PDA by reprogramming of macrophages that leads to conventional $CD4^+$ and $CD8^+$ T-cell activation. This work thus describes a critical new cellular entity in the landscape of the TME and suggests that iαβTs can be utilized for adoptive cell therapy or as targets of activation for immune-based therapies *in situ* in PDA.

METHODS

Animals and In Vivo Procedures

C57BL/6 (H-2Kb), B6.MRL-Fas^{lpr}/J, Dectin-1$^{-/-}$, CCR2$^{-/-}$, CCR5$^{-/-}$, CCR6$^{-/-}$, β2m$^{-/-}$, MHCII$^{-/-}$, OT-II, and CD45.1 mice were purchased from The Jackson Labs and bred in-house. KC mice, which express *Kras*^{G12D} in the progenitor cells of the pancreas, were a gift of Dafna Bar-Sagi of New York University (1). Both male and female mice were used, but animals were gender-matched within each experiment. For orthotopic pancreatic tumor challenge, 8- to 10-week-old mice were administered intrapancreatic injections of FC1242 tumor cells derived from KPC mice, as we previously described (5). In select experiments, we utilized KPC tumor cells, which we engineered to express Ovalbumin using the pCIneo-OVA vector (Addgene). PDA cells (1×10^5) were suspended in PBS with 50% Matrigel (BD Biosciences) and were injected into the body of the pancreas via laparotomy. Mice were sacrificed 3 weeks later for analysis. Alternatively, PDA cells (3×10^5) were implanted subcutaneously and tumor growth was serially measured. In some experiments, iαβTs or macrophages were mixed with tumor cells in a 1:3 ratio before orthotopic or subcutaneous injection. In other experiments, iαβTs were harvested by FACS and administered intravenously (5×10^6) twice weekly to orthotopic PDA-bearing mice beginning on day 5 after tumor implantation. For tracking experiments, iαβTs from CD45.1 hosts were coinjected with PDA cells into pancreata of CD45.2 mice and harvested 96 hours later. In select experiments, animals were treated with neutralizing mAbs directed against CD4 (GK1.5), CD8 (Lyt 2.1), F4/80 (CI:A3-1), TCRγ/δ (UC3-10A6), NK1.1 (PK136), and PD-L1 (10F.9G2; all Bio X Cell) using regimens we have previously described (5, 10). Alternatively, mice were treated with an agonizing ICOS mAb (7E.17G9, 100 μg, days 4, 7, and 10 after tumor challenge; Bio X Cell) or TLR4 ligand (LPS, 5 μg, intraperitoneally, 3×/week; Invivogen). Antimicrobial ablation was performed as previously described (10). Briefly, mice were administered an antibiotic cocktail by oral gavage daily for 5 consecutive days. Controls were gavaged with PBS. The oral gavage cocktail contained vancomycin (50 mg/mL; Sigma), neomycin (10 mg/mL; Sigma), metronidazole (100 mg/mL; Santa Cruz Biotech), and amphotericin (1 mg/mL; MP Biomedicals). Additionally, for the duration of the experiments, mouse drinking water was mixed with ampicillin (1 mg/mL; Santa Cruz Biotech), vancomycin (0.5 mg/mL; Sigma), neomycin (0.5 mg/mL; Sigma), metronidazole (1 mg/mL; Santa Cruz Biotech), and amphotericin (0.5 μg/mL; MP Biomedicals). All studies were approved by the New York University School of Medicine Institutional Animal Care and Use Committee.

Sequential IHC, Image Acquisition, and Processing for Human Tissues

Human tissues used for IHC analysis were obtained with written informed consent in accordance with the Declaration of Helsinki and were acquired through the Oregon Pancreas Tissue Registry. All studies were approved by an Institutional Review Board (IRB) under Oregon Health and Science University IRB protocol #3609. Human PDA and murine orthotopic PDA tissues were fixed with 10% buffered formalin, dehydrated in ethanol, and embedded with paraffin. Sequential IHC was performed on 5-μm formalin-fixed, paraffin-embedded (FFPE) sections using an adapted protocol based on methodology we previously described (27). Briefly, slides were deparaffinized and stained with hematoxylin (S3301, Dako), followed by whole-slide scanning at 20× magnification on an Aperio AT2 (Leica Biosystems). Tissues then underwent 15 minutes of heat-mediated antigen retrieval in pH 6.0 Citra solution (BioGenex), followed by 20 minutes of endogenous peroxidase blocking in 0.6% H_2O_2 (mouse) or 10 minutes of blocking in Dako Dual Endogenous Enzyme Block (S2003, Dako; human), then 10 minutes of protein blocking with 5% normal goat serum and 2.5% BSA in TBST. For staining of mouse tissue, primary antibody incubations were carried out overnight at 4°C with CD4 (D7D2Z, 1:50, Cell Signaling Technology), CD3 (SP7, 1:300, Thermo Fisher), and CD8 (4SM15, 1:100, eBioscience). For staining of human tissues, primary antibody incubations were carried out for 30 minutes at room temperature using CD4 (SP35, 1:4, Ventana), CD68 (PG-M1, 1:50, Abcam), CD3 (SP7, 1:150, Thermo Fisher), and Pan Cytokeratin (AE1/AE3, 1:2000, Abcam), and 60 minutes at room temperature using CD45 (HI30, 1:100, Thermo Fisher). After washing off primary antibody in TBST, either anti-rat, anti-mouse, or anti-rabbit Histofine Simple Stain MAX PO horseradish peroxidase (HRP)–conjugated polymer (Nichirei Biosciences) was applied for 30 minutes at room temperature, followed by AEC chromogen (Vector Laboratories). Slides were digitally scanned following each chromogen development, and the staining process was repeated starting at the Citra step for all subsequent staining cycles.

Scanned images were registered in MATLAB version R2018b using the SURF algorithm in the Computer Vision Toolbox (The MathWorks, Inc.). Image processing and cell quantification were performed using FIJI (FIJI Is Just ImageJ; ref. 28), CellProfiler Version 3.5.1 (29), and FCS Express 6 Image Cytometry RUO (De Novo Software). AEC signal was extracted for quantification and visualization in FIJI using a custom macro for color deconvolution. Briefly, the FIJI plugin Color_Deconvolution (H AEC) was used to separate hematoxylin, followed by post-processing steps for signal cleaning and background elimination. AEC signal was extracted in FIJI using the NIH plugin RGB_to_CMYK. For visualization, signal-extracted images were overlaid in pseudocolor in FIJI. Color deconvoluted images were processed in CellProfiler to quantify single-cell mean intensity signal measurements for every stained marker, and human T cells were identified and quantified by image cytometry in FCS Express based on the expression of known markers as follows: pan cytokeratin^{-} CD45^{+} CD68^{-} CD3^{+}, CD4$^{+/-}$, CD8$^{+/-}$.

Murine and Human Cellular Isolation, Flow Cytometry, and FACS

Single-cell suspensions of mouse PDA tumors were prepared for flow cytometry as described previously, with slight modifications (5). Briefly, pancreata were placed in cold 2% FACS (PBS with 2% FBS) with collagenase IV (1 mg/mL; Worthington Biochemical), Trypsin inhibitor (1 mg/mL; EMD Millipore), and DNase I (2 U/mL; Promega), and minced with scissors to submillimeter pieces. Tissues were then incubated at 37°C for 20 minutes with gentle shaking every 5 minutes. Specimens were passed through a 70-μm mesh and centrifuged at $350 \times g$ for 5 minutes. Splenocytes and thymocytes were prepared by manual disruption, as we described (5). Cell pellets were resuspended and cell labeling was performed after blocking FcγRIII/II with an anti-CD16/CD32 mAb (eBioscience) by incubating 1×10^6 cells with 1 μg of fluorescently conjugated mAbs directed against mouse CD45 (30-F11), CD3 (17A2), CD4 (RM4-5), CD8 (53-6.7), TCRβ (H57-597), CD62L (MEL-14), FasL (MFL3), NK1.1 (PK136), CD39 (Duha59), CCR2 (K036C2), CCR5 (HM-CCR5), CCR6 (292L17), CD44 (IM7), CD206 (C068C2), CD107a (1D4B), JAML (4E10), CD86 (GL1), Gr1 (RB6-8C5), MHCII (M5/114.15.2), PD-1 (29F.1A12), ICOS (15F9), TNFα (MP6-XT22), IL17A (TC11-18H10.1), TGFβ (TW7-16B4), LFA-1 (H155-78), IL10 (JES5-16E3), IFNγ (XMG1.2), Granzyme B (2-8898-80), PD-L1 (10F.9G2), B7-2 (PO3), CTLA4 (UC10-4B9), TIM3 (RMT3-23), CD40L (24–31), LAG3 (C9B7W), TLR4 (UT41), CD73 (TY/11.8), TGFβ (TW7-16B4), Dectin-1 (RH1), Ki67 (16A8), IL6 (MP5-20F3), TCR Vβ7 (TR310), TCR Vβ2 (B20.6), α-GalCer:CD1d complex (L363), pSTAT1 (A15158B; all BioLegend), CD45.1 (A20), RORγt (AFKJS-9), Perforin (eBioOMAK-D), T-bet (eBio4B10), and FOXP3 (FJK-16s; all eBioscience). Tetramer staining was performed as previously described, using a murine MR1-specific tetramer courtesy of the NIH Core Tetramer Facility (30). Intracellular staining was performed using the FOXP3 Fixation/Permeabilization Solution

Kit (eBioscience). Ova-specific CD8$^+$ T cells were identified using a SIINFEKL Pentamer (ProImmune). Mouse bone marrow–derived macrophages were generated as we described (31). Human pancreatic tumors and PBMCs were collected under an IRB-approved protocol. Human pancreatic leukocytes were prepared in a similar manner to that of mice. PBMCs were isolated by overlaying whole blood diluted 1:1 in PBS over an equal amount of Ficoll (GE Healthcare). Cells were then spun at 2,200 rpm, and the buffy coat was harvested, as we have described (32). Human PBMC macrophages were cultured plated in complete RPMI containing human FBS supplemented with human GM-CSF (2 μg/mL) and left in culture for 3 days until used in experiments. Analysis of human cells was performed using fluorescently conjugated antibodies directed against CD45 (2DI), TCRαβ cells (IP26), CD4 (A161A1), CD8 (HIT1A), TCR Vα7.2 (3C10), and CD56 (HCD56; all BioLegend). Dead cells were excluded from analysis using zombie yellow (BioLegend). Flow cytometry was performed on the LSR-II (BD Biosciences) or Attune NxT Flow Cytometer (Thermo Fisher). FACS sorting was performed on the SY3200 (Sony). Data were analyzed using FlowJo (Treestar). Chemokine and cytokine levels in cell culture supernatant were analyzed using Legendplex arrays, as per the manufacturer's protocol (BioLegend).

Coculture and In Vitro Experiments

For mouse or human macrophage polarization assays, iαβTs were cocultured with naïve splenic or PMBC-derived macrophages, respectively, for 36 hours in a 1:4 ratio. In select experiments, 36-hour conditioned media from iαβTs were added to macrophage cultures. In some experiments, a CCR5 small-molecule inhibitor or vehicle was added to the coculture well (Maraviroc, 20 μmol/L; Tocris Biosciences). Alternatively, iαβTs were cultured alone and treated with either Dectin-1 ligand (depleted zymosan, 10 μg/mL; Invivogen) or ICOSL Fc (10 μg/mL; Novoprotein). iαβT-KPC cell coculture experiments were performed in various ratios for 24 hours. Tumor cell proliferation was measured using the XTT assay kit according to the manufacturer's protocol (Sigma). Tumor cell lysis was measured using an LDH Cytotoxicity Assay Kit (Pierce) and apoptosis was determined using Annexin V and propidium iodide staining (both BioLegend). For antibody-based T-cell proliferation assays, T cells were activated using CD3/CD28 coligation in 96-well plates, as we previously described (5). Alternatively, cells were activated using αGalCer (0.1 μg/mL) in 96-well plates, as we described (33). For antigen-restricted T-cell stimulation assays, CD4$^+$ OT-II T cells were cultured with macrophages pulsed with Ova$_{323-339}$ peptide in a 5:1 ratio. T-cell activation was determined at 72 hours by flow cytometry. In selected wells, iαβTs were added to T-cell activation assays in a 1:4 ratio. TGFβ (AF-101-NA) and PD-L1 (10F.9G2, both 10 μg/mL; R&D Systems) were selectively neutralized in these assays.

FISH

The EUB338 16S rRNA gene probe labeled with the fluorophore Cy3 (extinction wavelength, 555 nm; emission wavelength, 570 nm; Molecular Probes) was used to detect the bacterial colonization within mouse pancreatic tissues by FISH. Fluorescence microscopic analysis was conducted with Nikon Eclipse 90i confocal microscope (Nikon) using a Cy3-labeled probe at 50 pmol/mL as described (34–36).

PCR Analysis

Genomic DNA was extracted using a DNAeasy mini kit (Qiagen). PCR was performed in duplicate for each sample using the BioRad Real-Time PCR System (BioRad). The primer sequence for *Ova* was F-GTGTTTAGCTCTTCAGCCAATCT, R-CTGCATGGACAGCTTGA GATA. Amplified PCR products were evaluated by agarose gel electrophoresis and subsequent ethidium bromide staining.

Sequential IHC and Image Acquisition

For histologic analysis, murine orthotopic PDA tissues were fixed with 10% buffered formalin, dehydrated in ethanol, and embedded with paraffin. Sequential IHC was performed on 5-μm FFPE murine PDA using a staining methodology we previously described (27). Briefly, slides were deparaffinized and stained with hematoxylin (S3301, Dako), followed by whole-tissue scanning at 20× magnification on an Aperio AT2 (Leica Biosystems). Slides then underwent 20 minutes of endogenous peroxidase blocking in 0.6% H_2O_2 followed by 15 minutes of heat-mediated antigen retrieval in pH 6.0 Citra solution (BioGenex), followed by 10 minutes of protein blocking with 5% normal goat serum and 2.5% BSA in TBST. Primary antibody incubations were carried out overnight at 4°C using rabbit anti-CD4 (D7D2Z, 1:50, Cell Signaling Technology), rabbit anti-CD3 (SP7, 1:300, Thermo Fisher), and rat anti-CD8 (4SM15, 1:100, eBioscience). After washing off primary antibody in TBST, either anti-rat or anti-rabbit Histofine Simple Stain MAX PO HRP-conjugated polymer (Nichirei Biosciences) was applied for 30 minutes at room temperature, followed by AEC chromagen (Vector Laboratories). Slides were digitally scanned following chromagen development, and the staining process was repeated starting at Citra step for all subsequent staining cycles. Images were coregistered using MATLAB software, followed by AEC color deconvolution and pseudocoloring in Fiji software.

Single-Cell RNA-seq Data Preprocessing

Sequencing results were demultiplexed and converted to FASTQ format using Illumina bcl2fastq software. The Cell Ranger Single-Cell Software Suite (https://support.10xgenomics.com/single-cell-gene-expression/software/pipelines/latest/what-is-cell-ranger) was used to perform sample demultiplexing, barcode processing, and single-cell 3′ gene counting. The cDNA insert was aligned to the mm10/GRCm38 reference genome. Only confidently mapped non-PCR duplicates with valid barcodes and UMIs were used to generate the gene-barcode matrix. Further analysis including the identification of highly variable genes, dimensionality reduction, standard unsupervised clustering algorithms, and the discovery of differentially expressed genes was performed using the Seurat R package (37). To exclude low-quality cells, cells that were extreme outliers in terms of library complexity, or cells that may possibly be multiple cells or doublets, we calculated the distribution of genes detected per cell and removed any cells in the top and bottom 2% quantiles. We additionally removed cells with more than 10% of the transcripts coming from mitochondrial genes.

Integrated Analysis of Single-Cell Data Sets

To account for technical batch differences between the three libraries, we utilized the Seurat alignment method for data integration, which specifically does not expect that confounding variables have uniform effects on all cells in a data set and allows for global transcriptional shifts between data sets. Seurat uses a variant of canonical correlation analysis (CCA) to find linear combinations of features and identifies shared correlation structures across data sets. For each data set, we identified variable genes, while controlling for the strong relationship between variability and average expression. We took the union of the top 2,000 genes with the highest dispersion from both data sets and ran a CCA to determine the common sources of variation between data sets. We then aligned the subspaces based on the first 15 canonical correlation vectors, generating a new dimensionality reduction that was then used for further analysis. For single-cell analysis of lymphocytes in PDA, from an unbiased pool of CD45$^+$ tumor-infiltrating leukocytes, we refined our analysis to include CD3d/CD3de expressing cells that expressed >1,000 detected genes. We then normalized the data by the total expression, multiplied this by a scale factor of 10,000, and log-transformed the result. The final data set included 807 cells with a median of 1,530 detected genes. For analysis of the total leukocyte population in tumors treated with iαβTs, we normalized the data by the total expression, multiplied this by a scale factor of 10,000, and log-transformed the result. The final data set included 3,839 cells with a median of 1,148 detected genes.

Visualization and Clustering of Single-Cell RNA-seq Data

To visualize the data, we further reduced the dimensionality of the data set to project the cells in two-dimensional space using principal component analysis followed by t-distributed stochastic neighbor embedding (t-SNE) based on the aligned CCA. Aligned CCA was also used as a basis for partitioning the data set into clusters using a smart local moving community detection algorithm (https://arxiv.org/ftp/arxiv/papers/1308/1308.6604.pdf). To find markers that define individual clusters, we performed differential expression analysis using Wilcoxon rank sum test for each cluster compared with all other cells for genes detected in at least 20% of the cluster cells. The initial analysis of PDA-infiltrating lymphocytes yielded seven clusters. We assigned cell-type identities based on the expression of known population markers as follows: PD-1^{hi}CD8^{+} T cells: *Pdcd1*^{hi}*Cd4*^{lo} *Cd8a*^{hi}*Ccl1*^{hi}; PD1^{lo}CD8^{+} T cells: *Pdcd1*^{lo}*Cd4*^{lo}*Cd8a*^{hi}*Ccl1*^{lo}*Ccl5*^{hi}; CD4^{+} T cells: *Cd4*^{hi}*Cd8a*^{lo}*Cd74*^{hi}*Pdcd4*^{hi}; iαβTs: *Cd4*^{lo}*Cd8a*^{lo}*Ccr7*^{hi} *Il2rb*^{lo} *Nkg7*^{lo} *Klrd1*^{lo} *Klrc2*^{lo}; NKT cells: *Cd4*^{lo}*Cd8a*^{lo}*Nkg7*^{hi} *Klrc2*^{hi}; γδ T cells: *Tcrg-c2*^{hi} *Cd4*^{lo}*Cd8a*^{lo}*Cd8b*^{med} *Gzma*^{hi}*Ccl5*^{hi}; Pro-B cells: *Ccnb2*^{hi}*Hmgb2*^{hi}*Stmn1*^{hi} *Cd3d*^{lo}. The initial analysis for the tumor-infiltrating leukocytes consisted of 14 clusters. We then assigned them cell-type identities based on the expression of known population markers, identifying 10 distinct populations in the following manner: T cells: *Cd3d*^{hi}*Cd3g*^{hi} *Cd3e*^{hi}*Cd4*^{hi}*Cd8a*^{hi}; B cells: *Cd19*^{hi} *Ebf1*^{hi}; iαβTs: *Cd3d*^{hi}*Cd3g*^{hi} *Cd3e*^{hi}*Cd4*^{lo}*Cd8a*^{lo}*Ly6c1*^{hi} *Klrk1*^{lo} *Klra7*^{lo}; NKT cells: *Cd3d*^{hi}*Cd3g*^{hi} *Cd3e*^{hi} *Klrk1*^{hi} *Klra7*^{hi}; NK cells: *Cd3d*^{lo}*Cd3g*^{lo} *Cd3e*^{lo}*Klrk1*^{hi} *Klra7*^{hi}; macrophages: *Itgam*^{hi}*Adgre1*^{hi}*Cd177*^{lo}; CX3CR1^{+} macrophages: *Itgam*^{hi}*Adgre1*^{hi} *Cx3cr1*^{hi}; CD103^{hi} MHCII^{hi}: *Itgae*^{hi}*H2-Ab1*^{hi}*CD74*^{hi}*Itgam*^{lo}; Batf3^{hi} MHCII^{hi}: *Batf3*^{hi} *CD74*^{hi}*H2-Ab1*^{hi} *Itgax*^{lo}*Itgam*^{lo}; neutrophils: *Cd177*^{hi} *Itgam*^{hi}. GSEA was performed on differentially expressed genes in the macrophage cluster. Upregulated and downregulated sets of genes were ranked based on their average and normalized log2 fold change between treatment and control group, and each gene set was assessed for enrichment in the KEGG_2016 gene set library (http://amp.pharm.mssm.edu/Enrichr/#stats) using python package gseapy (https://pypi.org/project/gseapy/) for analyses.

PDOTS Preparation, Treatment, and Analysis

PDOTS were prepared as we previously described, with slight modifications (38). Briefly, human surgically resected tumor specimens were received fresh in DMEM on ice and minced in 10-cm dishes. Minced tumors were resuspended in DMEM + 10% FBS with 100 U/mL collagenase type IV to obtain spheroids. Partially digested samples were pelleted and then resuspended in fresh DMEM + 10% FBS and strained over both 100-mm and 40-mm filters to generate S1 (>100 mm), S2 (40–100 mm), and S3 (<40 mm) spheroid fractions, which were subsequently maintained in ultra-low-attachment tissue culture plates. An aliquot of the S2 fraction was pelleted and resuspended in type I rat tail collagen and mixed with PBMC-derived allogeneic iαβTs that had been FACS sorted and activated overnight. This spheroid-iαβT mixture was then injected into the center gel region of the DAX-1 3-D microfluidic cell culture chip. Control spheroids were also plated (Aim Biotech). After 30 minutes at 37° C, collagen hydrogels containing PDOTS were hydrated with media in the side channels. After 72 hours, spheroids were digested with collagenase and single-cell suspensions were generated for flow cytometry. Fluorescently labeled antibodies for CD45 (2D1), TCRαβ (IP26), CD4 (A161A1), CD8 (HIT1a), HLA-DR (L243), TNFα (Mab11), CD11B (ICR F44), IFNγ (4S.B3), IL10 (JES3-9D7), ICOS (C398.4A), CD3 (OKT3), CD44 (IM7; all BioLegend), and CD86 (2331FUN-1; BD Biosciences) were used to stain for analysis. Human biological samples were sourced ethically, and their research use was in accord with the terms of the informed consents under an IRB-approved protocol.

T-cell Receptor Sequencing

CD4^{+}, CD8^{+}, and iαβTs were isolated by FACS, and genomic DNA was extracted using a DNAeasy mini kit (Qiagen). Mouse TCR sequencing was performed using the immunoSEQ Assay (Adaptive Biotechnologies). V, D, and J segments of the TCR were identified by multiplex PCR using forward primers in each V segment and reverse primers in each J segment. Detected template reads were normalized to total DNA content. Assessment of T-cell clonality and sequence overlap analyses were performed on immunoSEQ ANALYZER 3.0 software (Adaptive Biotechnologies).

Statistical Analysis

Data are presented as mean ± standard error. Statistical significance was determined by the Student *t* test and the log-rank test using GraphPad Prism 7 (GraphPad Software). P values ≤0.05 were considered statistically significant. Significance for GSEA and differential gene expression based on single-cell RNA-seq was determined using the Wilcoxon rank sum test with Bonferroni multiple-comparison correction.

Disclosure of Potential Conflicts of Interest

D. Saxena has ownership interest (including stock, patents, etc.) in Periomicscare LLC. L.M. Coussens reports receiving commercial research grants from Acerta Pharma, LLC, Deciphera Pharmaceuticals, Roche Glycart AG, and Syndax Pharmaceuticals, Inc.; reports receiving other commercial research support from Plexxikon Inc, Pharmacyclics, Inc., Acerta Pharma, LLC, Deciphera Pharmaceuticals, Genentech, Inc., Roche Glycart AG, Cell Signaling Technologies, and NanoString Technologies, Inc.; is a member of the Pharmacyclics, Inc. steering committee for PCYC-1137-CA (NCT02436668); and is a consultant/advisory board member for Syndax Pharmaceuticals, Inc., Cancer Research Institute (CRI), The V Foundation for Cancer Research, Cancer Research United Kingdom (CRUK) Early Detection (EDx) Research Committee, Starr Cancer Consortium, NIH/NCI-Frederick National Laboratory Advisory Committee (FNLAC), Cell Signaling Technologies, Carisma Therapeutics Inc., Verseau Therapeutics, Inc., Zymeworks, Inc., (P30) Melvin and Bren Simon Cancer Center, Indiana University, (P30) Koch Institute for Integrated Cancer Research, Massachusetts Institute of Technology, (P30) Salk Institute Cancer Center, Bloomberg-Kimmel Institute for Cancer Immunotherapy, Sidney Kimmel Comprehensive Cancer Center at Johns Hopkins, and Dana-Farber Cancer Center Breast SPORE. No potential conflicts of interest were disclosed by the other authors.

Authors' Contributions

Conception and design: M. Hundeyin, E. Kurz, J. Leinwand, B. Wadowski, G. Miller

Development of methodology: M. Hundeyin, E. Kurz, A. Mishra, J.A. Kochen Rossi, K.R. Leis, A. Ogunsakin, S. Savadkar, K.-K. Wong, L.M. Coussens, G. Miller

Acquisition of data (provided animals, acquired and managed patients, provided facilities, etc.): M. Hundeyin, E. Kurz, A. Mishra, J.A. Kochen Rossi, S.M. Liudahl, H. Mehrotra, L.E. Torres, J. Link, R.C. Sears, S. Savadkar, B. Aykut, M. Gelas, J. Lish, K. Chin, B. Wadowski, D.O. Adeegbe, S. Pushalkar, D. Saxena, K.-K. Wong, L.M. Coussens

Analysis and interpretation of data (e.g., statistical analysis, biostatistics, computational analysis): M. Hundeyin, E. Kurz, A. Mishra, S.M. Liudahl, M. Kim, L.E. Torres, S. Sivagnanam,

J. Goecks, K.M.S. Islam, I. Dolgalev, W. Wang, B. Aykut, J. Leinwand, M. Israr, M. Gelas, S. Shah, S. Pushalkar, V. Vasudevaraja, D. Saxena, L.M. Coussens, G. Miller

Writing, review, and/or revision of the manuscript: M. Hundeyin, E. Kurz, A. Mishra, L.E. Torres, B. Aykut, J. Leinwand, B. Diskin, M. Israr, D.O. Adeegbe, S. Pushalkar, D. Saxena, K.-K. Wong, L.M. Coussens, G. Miller

Administrative, technical, or material support (i.e., reporting or organizing data, constructing databases): M. Hundeyin, A. Mishra, L.E. Torres, A. Ogunsakin, K.M.S. Islam, S. Savadkar, W. Wang, S. Adam, M. Israr, M.S. Farooq, B. Wadowski, J. Wu, S. Shah, D. Saxena, L.M. Coussens

Study supervision: M. Hundeyin, E. Kurz, G. Miller

Acknowledgments

This work was supported by NIH grants CA168611 (G. Miller), CA203105 (G. Miller), CA215471 (G. Miller), CA19311 (G. Miller), and DK106025 (G. Miller), the Knight Cancer Institute NCI P30 CA069533 (L.M. Coussens and R.C. Sears), the Brenden-Colson Center for Pancreatic Care (L.M. Coussens, S.M. Liudahl, K.R. Leis, J. Link, R.C. Sears, S. Sivagnanam, J. Goecks), Stand Up To Cancer–Lustgarten Foundation, Pancreatic Cancer Convergence Dream Team Translational Research Grant (SU2-AACR-DT14-14; L.M. Coussens and S.M. Liudahl), Stand Up To Cancer (SU2C) is a Division of the Entertainment Industry Foundation administered by the American Association for Cancer Research, the Scientific Partner of SU2C; and a resident research fellowship from the American Society for Colorectal Surgery (M. Hundeyin).

Received February 5, 2019; revised May 14, 2019; accepted June 27, 2019; published first July 2, 2019.

REFERENCES

1. Guerra C, Schuhmacher AJ, Canamero M, Grippo PJ, Verdaguer L, Perez-Gallego L, et al. Chronic pancreatitis is essential for induction of pancreatic ductal adenocarcinoma by K-Ras oncogenes in adult mice. Cancer Cell 2007;11:291–302.
2. Biswas SK, Mantovani A. Macrophage plasticity and interaction with lymphocyte subsets: cancer as a paradigm. Nat Immunol 2010;11: 889–96.
3. DeNardo DG, Barreto JB, Andreu P, Vasquez L, Tawfik D, Kolhatkar N, et al. CD4(+) T cells regulate pulmonary metastasis of mammary carcinomas by enhancing protumor properties of macrophages. Cancer Cell 2009;16:91–102.
4. Jang JE, Hajdu CH, Liot C, Miller G, Dustin ML, Bar-Sagi D. Cross-talk between regulatory T cells and tumor-associated dendritic cells negates anti-tumor immunity in pancreatic cancer. Cell Rep 2017; 20:558–71.
5. Daley D, Zambirinis CP, Seifert L, Akkad N, Mohan N, Werba G, et al. gammadelta T cells support pancreatic oncogenesis by restraining alphabeta T cell activation. Cell 2016;166:1485–99.
6. Janakiram NB, Mohammed A, Bryant T, Ritchie R, Stratton N, Jackson L, et al. Loss of natural killer T cells promotes pancreatic cancer in LSL-Kras(G12D/+) mice. Immunology 2017;152:36–51.
7. Balomenos D, Shokri R, Daszkiewicz L, Vazquez-Mateo C, Martinez AC. On how Fas apoptosis-independent pathways drive T cell hyperproliferation and lymphadenopathy in lpr mice. Front Immunol 2017; 8:237.
8. Jiang X, Seo YD, Chang JH, Coveler A, Nigjeh EN, Pan S, et al. Long-lived pancreatic ductal adenocarcinoma slice cultures enable precise study of the immune microenvironment. Oncoimmunology 2017;6:e1333210.
9. Rao R, Graffeo CS, Gulati R, Jamal M, Narayan S, Zambirinis CP, et al. Interleukin 17-producing γδT cells promote hepatic regeneration in mice. Gastroenterology 2014;147:473–84.
10. Pushalkar S, Hundeyin M, Daley D, Zambirinis CP, Kurz E, Mishra A, et al. The pancreatic cancer microbiome promotes oncogenesis by induction of innate and adaptive immune suppression. Cancer Discov 2018;8:403–16.
11. Reikvam DH, Erofeev A, Sandvik A, Grcic V, Jahnsen FL, Gaustad P, et al. Depletion of murine intestinal microbiota: effects on gut mucosa and epithelial gene expression. PloS one 2011;6:e17996.
12. Ochi A, Nguyen AH, Bedrosian AS, Mushlin HM, Zarbakhsh S, Barilla R, et al. MyD88 inhibition amplifies dendritic cell capacity to promote pancreatic carcinogenesis via Th2 cells. J Exp Med 2012; 209:1671–87.
13. Jenkins RW, Aref AR, Lizotte PH, Ivanova E, Stinson S, Zhou CW, et al. Ex vivo profiling of PD-1 blockade using organotypic tumor spheroids. Cancer Discov 2018;8:196–215.
14. Seifert L, Werba G, Tiwari S, Giao Ly NN, Alothman S, Alqunaibit D, et al. The necrosome promotes pancreatic oncogenesis via CXCL1 and Mincle-induced immune suppression. Nature 2016;532:245–9.
15. Wu L, LaRosa G, Kassam N, Gordon CJ, Heath H, Ruffing N, et al. Interaction of chemokine receptor CCR5 with its ligands: multiple domains for HIV-1 gp120 binding and a single domain for chemokine binding. J Exp Med 1997;186:1373–81.
16. Franciszkiewicz K, Salou M, Legoux F, Zhou Q, Cui Y, Bessoles S, et al. MHC class I-related molecule, MR1, and mucosal-associated invariant T cells. Immunological Reviews 2016;272:120–38.
17. Le Bourhis L, Martin E, Péguillet I, Guihot A, Froux N, Coré M, et al. Antimicrobial activity of mucosal-associated invariant T cells. Nat Immunol 2010;11:701.
18. van Wilgenburg B, Scherwitzl I, Hutchinson EC, Leng T, Kurioka A, Kulicke C, et al. MAIT cells are activated during human viral infections. Nat Commun 2016;7:11653.
19. Juvet SC, Zhang L. Double negative regulatory T cells in transplantation and autoimmunity: recent progress and future directions. J Mol Cell Biol 2012;4:48–58.
20. McAllister F, Bailey JM, Alsina J, Nirschl CJ, Sharma R, Fan H, et al. Oncogenic Kras activates a hematopoietic-to-epithelial IL-17 signaling axis in preinvasive pancreatic neoplasia. Cancer Cell 2014;25: 621–37.
21. Nywening TM, Wang-Gillam A, Sanford DE, Belt BA, Panni RZ, Cusworth BM, et al. Targeting tumour-associated macrophages with CCR2 inhibition in combination with FOLFIRINOX in patients with borderline resectable and locally advanced pancreatic cancer: a single-centre, open-label, dose-finding, non-randomised, phase 1b trial. Lancet Oncol 2016;17:651–62.
22. Voelkl S, Moore TV, Rehli M, Nishimura MI, Mackensen A, Fischer K. Characterization of MHC class-I restricted TCRalphabeta+ CD4- CD8- double negative T cells recognizing the gp100 antigen from a melanoma patient after gp100 vaccination. Cancer Immunol Immunother 2009;58:709–18.
23. Young KJ, Kay LS, Phillips MJ, Zhang L. Antitumor activity mediated by double-negative T cells. Cancer Res 2003;63:8014–21.
24. Daley D, Mani VR, Mohan N, Akkad N, Ochi A, Heindel DW, et al. Dectin 1 activation on macrophages by galectin 9 promotes pancreatic carcinoma and peritumoral immune tolerance. Nat Med 2017; 23:556–67.
25. Daley D, Mani VR, Mohan N, Akkad N, Pandian G, Savadkar S, et al. NLRP3 signaling drives macrophage-induced adaptive immune suppression in pancreatic carcinoma. J Exp Med 2017;214:1711–24.
26. Guerriero JL. Macrophages: the road less traveled, changing anticancer therapy. Trends Mol Med 2018;24:472–89.
27. Tsujikawa T, Kumar S, Borkar RN, Azimi V, Thibault G, Chang YH, et al. Quantitative multiplex immunohistochemistry reveals myeloid-inflamed tumor-immune complexity associated with poor prognosis. Cell Rep 2017;19:203–17.
28. Schindelin J, Arganda-Carreras I, Frise E, Kaynig V, Longair M, Pietzsch T, et al. Fiji: an open-source platform for biological-image analysis. Nat Methods 2012;9:676–82.
29. Carpenter AE, Jones TR, Lamprecht MR, Clarke C, Kang IH, Friman O, et al. CellProfiler: image analysis software for identifying and quantifying cell phenotypes. Genome Biol 2006;7:R100.

30. Corbett AJ, Eckle SBG, Birkinshaw RW, Liu L, Patel O, Mahony J, et al. T-cell activation by transitory neo-antigens derived from distinct microbial pathways. Nature 2014;509:361.
31. Wang W, Marinis JM, Beal AM, Savadkar S, Wu Y, Khan M, et al. RIP1 kinase drives macrophage-mediated adaptive immune tolerance in pancreatic cancer. Cancer Cell 2018;34:757–74.
32. Rehman A, Hemmert KC, Ochi A, Jamal M, Henning JR, Barilla R, et al. Role of fatty-acid synthesis in dendritic cell generation and function. J Immunol 2013;190:4640–9.
33. Ibrahim J, Nguyen AH, Rehman A, Ochi A, Jamal M, Graffeo CS, et al. Dendritic cell populations with different concentrations of lipid regulate tolerance and immunity in mouse and human liver. Gastroenterology 2012;143:1061–72.
34. Sunde PT, Olsen I, Gobel UB, Theegarten D, Winter S, Debelian GJ, et al. Fluorescence in situ hybridization (FISH) for direct visualization of bacteria in periapical lesions of asymptomatic root-filled teeth. Microbiology 2003;149:1095–102.
35. Thimm T, Tebbe CC. Protocol for rapid fluorescence in situ hybridization of bacteria in cryosections of microarthropods. Appl Environ Microbiol 2003;69:2875–8.
36. Choi YS, Kim YC, Baek KJ, Choi Y. In situ detection of bacteria within paraffin-embedded tissues using a digoxin-labeled DNA probe targeting 16S rRNA. J Visualized Exp 2015:e52836.
37. Butler A, Hoffman P, Smibert P, Papalexi E, Satija R. Integrating single-cell transcriptomic data across different conditions, technologies, and species. Nat Biotechnol 2018;36:411–20.
38. Jenkins RW, Aref AR, Lizotte PH, Ivanova E, Stinson S, Zhou CW, et al. Ex vivo profiling of PD-1 blockade using organotypic tumor spheroids. Cancer Discov 2018;8:196–215.